Fine-tuning spatial-temporal dynamics and surface receptor expression support plasma cell-intrinsic longevity

Zhixin Jing[1], Phillip Galbo[2,3], Luis Ovando[1], Megan Demouth[2], Skylar Welte[1], Rosa Park[1], Kartik Chandran[3], Yinghao Wu[3,4], Thomas MacCarthy[5], Deyou Zheng[2,4], David Fooksman[1,2]

Affiliations

[1] Department of Pathology, Albert Einstein College of Medicine, Bronx, NY 10461

[2] Department of Genetics, Albert Einstein College of Medicine, Bronx, NY 10461

[3] Department of Microbiology and Immunology, Albert Einstein College of Medicine, Bronx, NY 10461

[4] Department of System and Computational Biology, Albert Einstein College of Medicine, Bronx, NY 10461

[5] Department of Applied Mathematics and Statistics, Stony Brook University, Stony Brook, NY 11794

LEAD CONTACT

David Fooksman, David.fooksman@einsteinmed.edu

HIGHLIGHTS

- LLPCs have reduced motility and increased clustering in the BM
- LLPCs accumulate in the BM PC pool, with mouse age
- LLPCs have unique surfaceome, transcriptome, and BCR clonality
- CXCR4 controls maintenance of PCs and antibody titers

ABSTRACT (199 words)

Durable serological memory following vaccination is critically dependent on the production and survival of long-lived plasma cells (LLPCs). Yet, the factors that control LLPC specification and survival remain poorly resolved. Using intra-vital two-photon imaging, we find that in contrast to most plasma cells in the bone marrow, LLPCs are uniquely sessile and organized into clusters that are dependent on April, an important survival factor. Using deep, bulk RNA sequencing, and surface protein flow-based phenotyping, we find that LLPCs express a unique transcriptome and proteome compared to bulk PCs, fine tuning expression of key cell surface molecules, CD93, CD81, CXCR4, CD326, CD44 and CD48, important for adhesion and homing, and phenotypically label LLPCs within mature PC pool. Conditional deletion of *Cxcr4* in PCs following immunization leads to rapid mobilization from the BM, reduced survival of antigen-specific PCs, and ultimately accelerated decay of antibody titer. In naïve mice, the endogenous LLPCs BCR repertoire exhibits reduced diversity, reduced somatic mutations, and increased public clones and IgM isotypes, particularly in young mice, suggesting LLPC specification is non-random. As mice age, the BM PC compartment becomes enriched in LLPCs, which may outcompete and limit entry of new PC into the LLPC niche and pool.

INTRODUCTION

Prophylactic antibodies induced by vaccines provide rapid, systemic and in some cases, long-lasting immune protection against many infectious diseases. Variability in the duration of antibody responses is chiefly dependent on the composition of short-lived and long-lived plasma cells produced, which can have distinct lifespans of a few days and months or years in mice, respectively (Sze et al., 2000). The ability to generate LLPCs also declines with old age, and hence the durability of the vaccine response (Frasca and Blomberg, 2020) (Palacios-Pedrero et al., 2021). Therefore, understanding how LLPCs are generated and maintained are essential for enhancing durability of vaccine-induced antibody responses in humans.

Previous studies have reported these LLPCs are enriched in the bone marrow (BM) but can also be found in spleen and mucosa (Bohannon et al., 2016; Bortnick et al., 2012; Lemke et al., 2016; Manz et al., 1997; Slifka et al., 1998). Tracking of endogenous polyclonal LLPCs is challenging, requiring labeling and tracking by thymidine analogs like BrdU, or looking for antigen-specific antibody forming cells by ELISPOTs. However, these approaches are not amenable to tracking live cells by flow cytometry, as there have been no phenotypic markers for endogenous LLPCs, making these cells elusive. Approaches to genetically track LLPCs were recently established (Xu et al., 2020), which allows studying their turnover and generation.

One major question is how these cells are specified. LLPCs can mature from newly-minted plasmablasts (PBs) in the germinal center that have undergone affinity maturation (Phan et al., 2006; Takahashi et al., 1998). However, LLPCs can also develop in a T cell-independent manner (Bortnick and Allman, 2013), and B-1 lineages (Vergani et al., 2022), suggesting that there are multiple, distinct pathways to becoming LLPCs, or specification is regulated extrinsically by their niche, or both (Robinson et al., 2020). Thus, it is unclear if LLPCs arise from unique clones, unique pools of B cells or are just randomly specified from the bulk PC pool,

in a stochastic manner, potentially through maturation in the bone marrow niche. Determining what is required for LLPC specification is important for vaccine development.

A second major question regarding LLPCs is how they are maintained and survive in a cell-specific manner. While functionally they are metabolically active, quiescent, murine LLPCs (defined as B220- 2NBDG^{+}) are thought to have minimal transcriptional specificity compared to bulk PCs (Lam et al., 2018). In contrast, human LLPCs (CD19^{-} CD138^{high}) have been shown to be transcriptionally distinct from other mature PCs (Joyner et al., 2022) .

The BM is a major lodging site for LLPCs and it is believed that key cell-extrinsic cellular and molecular factors support their longevity. PCs migratory behavior and positioning within BM parenchyma is also linked to chemokine receptor signaling, cell adhesion, cytokine, and age of mice. Previous work from our laboratory found that as PCs age, CXCR4 expression is increased, suggesting LLPCs may upregulate certain key molecules for survival. CXCR4 is a master chemokine receptor for BM tropism but its role in humoral immunity is thought to be dispensable (Nie et al., 2004). However, CXCR4 drives PC motility in the BM and is upregulated on PC with aging (Benet et al., 2021). We and others have shown that BM PCs are spatially organized in clusters (Benet et al., 2021; Mokhtari et al., 2015) and PCs are less motile when they enter these clusters, suggesting extrinsic signals may be important cues for motility. Moreover, in mice lacking APRIL, a key survival cytokine for PCs, these clusters were reduced, suggesting clusters and cell dynamics may be functionally important for PC survival.

In this study, we aim to understand what unique features are associated with LLPC physiology, at a molecular, cellular, and spatial-temporal level using cell fate labeling of PCs. We find that these cells exhibit intrinsic changes in gene expression and cell motility patterns that may underlie their unique ability to persist for long periods of time, despite competition from a continuously evolving PC pool. Among the factors promoting their survival, CXCR4 plays a

dominant cell-intrinsic role in promoting LLPCs retention and survival and thus, maintaining durability of humoral responses.

EXPERIMENTAL MODEL AND SUBJECT DETAILS

Mice

Prdm1-EYFP (Fooksman et al., 2010) were generated previously and can also be obtained from the Jackson Laboratory. Rosa26-CAG-LSL-tdTomato (Ai14) (Madisen et al., 2010), Rosa26-LSL-EYFP (Srinivas et al., 2001), and *Cxcr4*$^{fl/fl}$ (Nie et al., 2004) were purchased from the Jackson Laboratory. C57BL/6 (CD45.2) and B6-Ly5.1/Cr (CD45.1) mice were purchased from Charles River. All mice were housed in groups of 2–5 animals per cage in SPF facilities at Albert Einstein College of Medicine. The animal protocol in this study was approved by Albert Einstein College of Medicine Institutional Animal Care Use Committee (IACUC). For PC turnover experiments, both females and males that are young (6-8 weeks old) or middle-aged (20-24 weeks old) were used. For mixed bone marrow chimera experiments, 6-8 weeks old sex-matched mice were used as hosts, and 16-24 weeks old WT or CXCR4^{cKO} mice were used as donors.

Blimp1-Cre^{ERT2}-IRES-TdTomato (BEC) mouse were constructed using CRISPR-Cas9 technology on the C57BL/6 background by knocking-in Cre^{ERT2}-IRES-TdTomato cassette downstream of the exon 6 of Prdm1 locus, targeted with one single guide RNA (TCTGTGGGCAGAAACCCGCG). Founders and F1 progenies were genotyped by PCR using primers (Integrated DNA Technologies) targeting Prdm1 genomic region (5'-GGCAAGATCAAGTATGAGTGC-3', Forward) and IRES sequence (5'-GCCAAAAGACGGCAATATGG-3', Reverse). This mouse line was backcrossed to C57BL/6 for

at least three generations. Since BEC is a knock-in knockout allele, only heterozygotes were used for all experiments.

Generation of mixed bone marrow chimera

6-8 weeks old CD45.1 recipient mice were lethally irradiated (950 RAD) and reconstituted with 7-8 x 10^6 50:50 mixture of WT:CXCR4^{cKO} total bone marrow cells, and allowed to recover for 8 weeks with Sulfamethoxazole and Trimethoprim (ANI Pharmaceutials) added to the drinking water (1:50 v/v) in the first 2 weeks post reconstitution.

Immunizations and treatments

For hapten-protein conjugate immunizations, WT or CXCR4^{cKO} mice were immunized intraperitoneally (i.p.) with 50 µg of $NP_{(32)}$-KLH (Biosearch Technologies) in PBS emulsified with alum (Imject Alum; Thermo Fisher Scientific) at 2:1 v:v ratio in 150 µl volume. For PC turnover experiments, 4 mg tamoxifen (MilliporeSigma) were administered by oral gavage per mouse for three consecutive days. For intratibial injection experiments, 5 µg of 4-Hydroxytamoxifen (MilliporeSigma) in 10 µl 5% ethanol (diluted with PBS) was given through shaved knee joint into the tibia using 29G insulin syringes, and 2.5 µg pertussis toxin (MilliporeSigma) in 100 µl volume PBS were intravenously (i.v.) injected to recipient mice. For glucose uptake experiments, 50 µg 2-NBDG (Thermo Fisher Scientific) in 100 µl volume PBS was i.v. injected into mix chimeric mice for exactly 15 min before sacrifice.

Flow cytometry

Single cell suspensions of bone marrow and spleen were resuspended in PBS containing 0.5% BSA and 1 mM EDTA and filtered through a 70 µm nylon mesh. Cells were blocked with anti-CD16/32 (2.4G2, Bio X Cell) and then stained for surface proteins with a combination of antibodies on ice for 30min, and analyzed on Cytek Aurora (Cytek Biosciences). Single stains for YFP and TdTomato were prepared using blood cells from Blimp1-YFP mouse and OT-II

TdTomato mouse, and all other stains were made by staining wildtype bone marrow cells with individual fluorescently labeled antibody. Compensations were done by automatic live unmix in SpectroFlo software (Cytek Biosciences) during acquisition, followed by manual adjustment of the compensation matrix. To ensure the accuracy of the manual changes in the compensation matrix, day 5 middle-aged BEC-YFP bone marrow cells were stained with each panel antibody separately to control for the matrix for each marker accordingly such that each stain consists of a basic panel including YFP, TdTomato, CD138-APC, B220-APCCy7, live/dead-CD4/8-BV510, and one of panel markers. Then, for each timepoint (except day 5) analyzed in the PC timestamping experiments, a day 5 middle-aged BEC-YFP mouse stained with all panel antibodies were included as a compensation control. The profiling of the total 19 markers were done by splitting into 3 subpanels with each panel sharing CD138-APC, B220-APCCy7, and live/dead-CD4/8-BV510. The antibody dilution was determined by titrating absolute amount (in μg) per million total bone marrow cells. For intracytoplasmic (4-hydroxy-3-nitrophenyl)acetyl (NP) staining in PCs, surface-stained cells were fixed and permeabilized using BD Cytofix/Cytoperm Fixation/Permeabilization kit (BD Biosciences), followed by NP-BSA-Fluorescein (Biosearch Tech) staining in 1:200 dilution for 1 hr at 4℃.

Anti-B220 (RA3-6B2), Bcl-2 (BCL/10C4), CD4 (GK1.5), CD8 (53-6.7), CD37 (Duno85), CD44 (IM7), CD45.2 (104), CD48 (HM48-1), CD81 (Eat-2), and CD98 (RL388) were purchased from Biolegend. CD28 (37.51), CD53 (OX-79), CD79b (HM79B), CD93 (AA4.1), CD126 (D7715A7), CD138 (281-2), CD147 (RL73), CD184 (2B11), CD267 (8F10), CD268 (7H22-E16), CD319 (4G2), CD326 (G8.8) were purchased from BD Biosciences. CD3e (145-2C11), CD45.1 (A20) and CD49d (R1-2) were purchased from Fisher Scientific. CD269 (REA550) was purchased from Miltenyi Biotec. Mcl-1 (D2W9E) was purchased from Cell Signaling Technology.

In-vitro assays

For NP-binding ELISA of mouse serum, high-binding 96 well plates (Corning Costar) were coated with 2 µg/ml NP-OVA (Biosearch Tech) in 50 µl volume bicarbonate/carbonate binding buffer (Abcam) overnight at 4℃. Parafilm were used to minimize evaporation of coating buffer inside the plate. Then coating buffer were removed and the plate was blocked with 200 µl PBS containing 1% BSA per well for 2 hrs at room temperature (RT). After removing blocking buffer, serum samples were added in 50 µl volume with starting dilution at 1:4000 (v:v in blocking buffer) for 4 serial 2-fold dilutions in triplicates, and anti-NP standard antibody (9T13) were added in 50 µl volume with starting concentration at 1 µg/ml for 8 serial 2-fold dilutions in duplicates, followed by incubation for 2 hrs at RT. The plates were washed 4 times with PBS containing 0.05% Tween (PBST) before adding 50 µl peroxidase goat anti-mouse IgG-HRP (Jackson ImmunoReseach) at 1:5000 dilution (v:v in blocking buffer) per well for 1 hr at RT. The plates were again washed 4 times with PBST, followed by adding 50 µl TMB substrate (MilliporeSigma) for 5-10 mins at RT, which is stopped by adding 25 µl sulfuric acid (Thermo Fisher Scientific). The plates were read by EMax Plus microplate reader (Molecular Devices) at 450 nm wavelength using SoftMax Pro 7 software.

Multiphoton intravital imaging and analysis

Surgical preparation for BM intra-tibial imaging was done as previously described (Benet et al., 2021). Mice were anesthetized using isoflurane gas during imaging process for 4-5 hours. Z-stack images for multiple regions of tibia were collected sequentially and stitched together either before or after long-term steady state intravital imaging using Olympus software. All imaging was performed using an Olympus FVE-1200 upright microscope, 25x1.04 NA objective, and Deepsee MaiTai Ti-Sapphire pulsed laser (Spectra-Physics) tuned to 920 nm. To maintain mouse body temperature and limit room light exposure, the microscope was fitted with custom-built incubator chamber and heated 37℃ platform. Time lapses were conducted every 3 mins as 100-120 µm deep Z-stacks (5 µm or 3 µm steps) with 1x zoom and with 512 x 512 X-Y

resolution. All image analysis was conducted using Imaris software 9.3 (Bitplane) to detect and track LLPCs ($YFP^{+}TdTomato^{bright}$) and bulk PCs ($YFP^{+}TdTomato^{dim}$) in young and middle-aged mice and to correct drift. Ratio channels (green over red, ch2/ch3) were created together with background subtraction from infrared channel (ch4) to separate LLPCs from bulk PCs.

Nearest neighbor analysis

LLPCs ($YFP^{+}TdTomato^{bright}$) and bulk PCs ($YFP^{+}TdTomato^{dim}$) in stitched z-stack images were detected as described above. The 2D position coordinates (X and Y) were generated from Imaris built-in spot's function. Nearest neighbor analysis program was created in Fortran using high performance computing. The average distance between individual LLPC spots and 20 nearest total PC spots (combining both LLPCs and bulk PCs), and between individual bulk PC spots and their 20 nearest total PC spots were calculated by the program. Then both LLPC spots and bulk PC spots were randomly picked and the sample size for each subset was determined using 95% confidence level, 5% margin of error, and total number of spots from each mouse inputted as population size. The random picking process was iterated twice per subset. The scripts were executed using a Fortran compiler (cygwin). All code of the data analysis and work flow can be viewed as text document files provided at github link: https://github.com/davidfooksman/nearest-neighbor/

RNA isolation and quantitative real-time RT-PCR

At least 20000 LLPCs ($YFP^{+}TdTomato^{+}$) and 80000 bulk PCs ($YFP^{-}TdTomato^{+}$) from bone marrow or spleen were sorted using Aria III (BD) for total RNA extraction using RNeasy Plus Mini Kit (Qiagen) according to manufacturer's protocol. 30 µl RNase-free water were loaded to the spin column membrane twice to reach higher RNA concentration. 4 µl RNA samples were used for reverse transcription using High-Capacity RNA-to-cDNA Kit (Applied Biosystems)

214 according to manufacturer's protocol. 2 µl cDNA from each sample were used for real time PCR
215 using TaqMan Universal Master Mix II with UNG (Applied Biosystems) according to
216 manufacturer's protocol. Predesigned TaqMan assays for Actb (Mm02619580_g1) and Cxcr4
217 (Mm01996749_s1) were purchased from Thermo Fisher Scientific.

218 **Bulk RNA sequencing cDNA library preparation**

219 Bone marrow and splenic PCs were isolated and enriched using $CD138^+$ Plasma Cell Isolation
220 Kit (Miltenyi Biotec), and stained for CD4 (GK1.5) and CD8 (53-6.7) to dump $TdTomato^+$ T cells
221 and DAPI for excluding dead cells before sorting on Aria III (BD) or MoFlo XDP (Beckman
222 Coulter) for RNA extraction. ~1000 $CD4^-CD8^-DAPI^-TdTomato^+$ cells from each enriched
223 samples were sorted into a PCR tube (USA Scientific) containing 0.5 µl 10x reaction buffer and
224 half the final volume of nuclease-free water provided in SMART-Seq v4 Ultra Low Input RNA Kit
225 for Sequencing (Takara Bio), and subsequent processes were following manufacturer's protocol.
226 All mixing steps were done by pipetting up and down 5-6 times. ERCC RNA Spike-In Control
227 Mixes (1:5000) (Life Technologies) were added to sorted cells together with lysis buffer.
228 Purification of amplified cDNA was done using Agencourt AMPure XP Kit (Beckman Coulter) on
229 a magnetic separation rack for 1.5 ml tubes (New England Biolabs). The concentration of
230 purified cDNA was determined using Qubit 1X dsDNA HS Assay Kit (Thermo Fisher Scientific)
231 on a Qubit 2.0 fluorometer (Thermo Fisher Scientific). The quality of purified cDNA was verified
232 on a 2100 Bioanalyzer (Agilent Technologies), and the average cDNA fragment size for a typical
233 PC sample was peaked at approximately 600 bp following a normal distribution pattern. Finally,
234 sequencing adaptors were added to using Nextera XT DNA Library Preparation Kit (Illumina)
235 following manufacturer's protocol. The library containing all samples was manually mixed to
236 ensure equal final concentration of all samples, and sent for next generation deep sequencing
237 by Genewiz/Azenta using NovaSeq S4 lane machine (Illumina) to reach an average of 50
238 million reads per sample.

RNA-seq data processing and analysis

RNA-seq reads were aligned to the mouse genome (mm39/GRCm39) using STAR aligner (v2.6.1b) (Dobin et al., 2013). Counts for individual genes were quantified using the RSEM program (v1.3.1) (Li and Dewey, 2011). Differential expression was computed using the DESeq2 (v 1.26.0), from pair-wise comparisons at adjusted p value < 0.05 (without additional fold change threshold) were collected, clustered by K-mean clustering (k=5), and used for Gene Ontology (GO) enrichment analysis with the patherdb.org server. Enriched GO at adjusted p < 0.05 were obtained and then differentially expressed genes in biologically relevant GO terms for each of the six comparisons were subject to over representation analysis by the Fisher's test, with the results shown as bubble plots. Raw data and processed files were uploaded to the NCBI server (GSE221251).

Transmission electron microscopy

PCs are isolated and enriched the same way as mentioned in the "Bulk RNA sequencing cDNA library preparation" section. 4000-8000 LLPCs ($YFP^{+}TdTomato^{+}$) and 40,000-200,000 bulk PCs ($YFP^{-}TdTomato^{+}$) were subsequently collected by sorting into a 500 µl low adhesion microcentrifuge tubes (USA Scientific) using Aria III (BD) or MoFlo XDP (Beckman Coulter), and 5-6 million sheep red blood cells (Innovative Research) were added to the same tube to provide contrast to the PCs, as previously described (Joyner CJ et al., 2021 Life Science Alliance), which were pelleted by centrifugation at 350g for 5 mins at RT. The supernatant was removed by aspiration, and the fixative containing 2.5% glutaraldehyde in 0.1M cacodylate (prewarmed at RT) was gently added by layering on top of the residual volume of buffer including the cell pellets for 15 mins at RT. Samples were postfixed with 1% osmium tetroxide followed by 2% uranyl acetate, dehydrated through a graded series of ethanol and embedded in LX112 resin (LADD Research Industries, Burlington VT). Ultrathin sections were cut on a Leica Ultracut UC7,

stained with uranyl acetate followed by lead citrate and viewed on a JEOL 1400 Plus transmission electron microscope at 120kv.

BCR repertoire analysis

BCR clones were inferred from RNA-Seq data, individually for each sample, using MIXCR v4.0.0b (Bolotin et al., 2015) using the following commands:

```
mixcr align -s mmu -p kAligner2
mixcr assemble --write-alignments
mixcr assembleContigs
mixcr exportClones -c IG -p fullImputed
```

The resulting clone files were pre-processed using a custom python script to separate IGH, IGK and IGL clones and to remove small clones of size <10. The resulting datasets were processed using the R package immunarch (https://immunarch.com/). Each repertoire (IGH, IGK, IGL) was loaded using repLoad. Diversity (Chao1) statistics were calculated using repDiversity and repertoire overlaps using repOverlap, For SHM estimates, we used custom R scripts. We filtered out fragmented (lists of sequences with commas), then processed the resulting sequences through IMGT-High V-Quest, which identifies mutations with respect to the closest germline sequence (from IMGT file "8_V-REGION-nt-mutation-statistics.txt"). To avoid double-counting of mutations within a clone, we selected a random sequence from each clone (most clones only had one sequence), then calculated the mean mutation frequency per sequence (number of mutations/V gene length), and then aggregated these to calculate a mean for each IGHV gene allele within each sample (e.g. the mean for all clones assigned to the IGHV8-9*01 allele). Pairwise statistical comparisons between the samples were performed using a paired t-test based on matching alleles (alleles that did not match were not used). Benjamini-Hochberg corrected P values were calculated using the R function p.adjust with the argument method="BH".

Quantification and statistical analyses

289 Statistical tests were performed using GraphPad Prism (v7 and v8). Specific tests used in each
290 figure are provided in the figure legends with asterisks for statistical significance (*, p-value ≤
291 0.05; **, p-value ≤ 0.01; ***, p-value ≤ 0.001; ****, p-value ≤ 0.0001) or "ns" denoting
292 comparisons that are not statistically significant. Data are presented as the mean ± SD or mean
293 ± SEM. For PC half-life ($t_{1/2}$) calculation, the procedure was done exactly as previously
294 described (Xu et al., 2020). For RT-qPCR analysis, $2^{-\Delta\Delta Ct}$ method was used to calculate the fold
295 change in *Cxcr4* gene expression relative to the expression of housekeeping gene *Actb* in WT
296 samples.

297

298

RESULTS

Plasma cell turnover rate decreases with mouse age

We previously reported that in middle-aged mice, PC motility and clustering within the BM and their recirculation capacity was increased, in comparison to young mice (Benet et al., 2021). We speculated that these changes in PC dynamics could alter homeostatic PC turnover rates and may also reflect changes in frequency of LLPCs within PC pool with aging. To study LLPC survival mechanisms, we constructed a novel mouse line, Blimp1-ERT2-Cre-TdTomato (BEC), which contains a tamoxifen-inducible cre recombinase (ERT2-cre) and fluorescent reporter TdTomato under the control of the *Prdm1* (BLIMP1) locus (Supplemental Figure 1A). We verified that >99% of $CD138^{high}$B220- BM PCs were $TdTomato^{+}$ (Supplemental Figure 1B) and that 94% of $TdTomato^{+}$ were ASCs ($CD138^{High}$) (Figure 1A, Supplemental Figure 1C). Tomato expression was about 1.5-2 log higher than Blimp-1 negative cells, similar to expression by other reporters in the *Prdm1* endogenous locus (Kallies et al., 2004; Liu et al., 2022; Robinson et al., 2022). To label and track lifespans of polyclonal PCs under steady-state conditions, we crossed allele BEC with Rosa26-LSL-EYFP conditional reporter (Srinivas et al., 2001) to generate BEC-YFP mouse. Acute treatment with tamoxifen for three consecutive days induced robust Cre-mediated recombination and irreversible expression of YFP, comprised of 98% PCs at day 5 (Figure 1A) but not in the absence of tamoxifen treatment (Figure 1B). Over time, YFP^{+} PCs that survive for months should by definition be bona fide LLPCs. However, in these mice, not all LLPCs would be YFP^{+}, as new LLPCs should develop in the unlabeled (YFP^{-}) fraction.

To study aged-related changes in PC turnover, naïve young (6-8 weeks old) and middle-aged (20-24 weeks old) BEC-YFP mice were acutely treated with tamoxifen and tracked over 150 days after treatment (Figure 1C). At day 5 post treatment, both age groups had similar frequency of YFP^{+} PCs in the BM (~65%) and in the spleen (~62%) (Figure 1D). However, over time, the remaining frequency of YFP^{+} cells of total PCs in young mice were significantly lower

than in middle-aged mice in both BM and spleen, indicating more PC turnover in the young mice. At day 150, only 1.8% BM PCs were YFP^+ in young mice compared to 14% in middle-aged mice, while in spleen, 0.6% YFP^+ PCs remained in young mice compared to 3.1% in middle-aged mice (Figure 1E-F). Based on absolute numbers of YFP^+ PCs, we analyzed rate of PC decay in the BM and spleen and found that BM PCs decay more rapidly in young mice ($t_{1/2}$ = 58 days) than in middle-aged mice ($t_{1/2}$ = 93 days) (Figure 1G). In the spleen decline of labeled PCs was overall faster than in the BM, in line with previous reports (Xu et al., 2020). However, we observed that the decline was slightly more rapid in young mice ($t_{1/2}$ = 28 days) as compared to middle-aged mice ($t_{1/2}$ = 39 days) (Figure 1H). Thus, we conclude that homeostatic PC turnover is dependent on tissue-specific microenvironment and aging, suggesting that LLPCs may accumulate with aging, particularly in the bone marrow.

BM LLPCs display cell-intrinsic arrest and clustering

Reduced PC turnover with age, specifically in the BM niche, suggested that PCs were more sessile and better retained in the BM with aging. However, our previous study that showed middle-aged mice had increased overall PC motility and recirculation compared to young mice (Benet et al., 2021). We hypothesized that in our previous study, imaging and recirculation measurements did not discriminate between behaviors of LLPCs and immature PCs, which may have different dynamics.

To test this idea, we applied BEC fate labeling to specifically track polyclonal LLPC dynamics and organization in the bone marrow of unimmunized mice. While YFP expression from Rosa26 reporter was bright enough to visualize labeled LLPCs, YFP^- bulk PCs, which also expressed low levels of Tomato from expression of the BEC allele ($Tomato^{dim}$), were insufficiently labeled for deep imaging in the BM. Thus, we bred double PC reporter, Blimp1-

YFP BEC *rosa26*$^{LSL\text{-}Tomato}$ mice, in which all PCs were YFP^{high} from expression of the Blimp1-YFP reporter, and with tamoxifen treatment, could be fate-labeled to co-express high levels of Tomato. We treated these mice with tamoxifen and analyzed surface phenotype of PCs at day 5 and 60 post treatment (Figure 2A). Tomato^{bright} labeled PCs were easily discernable from Tomato^{dim} bulk PCs by flow cytometry (Figure 2B). While at day 5 post treatment, Tomato^{bright} and Tomato^{dim} PCs were similar in PC maturation markers CXCR4 and CD93, by day 60, Tomato^{bright} were phenotypically distinct suggesting they had matured to a LLPC state (explored further in the next section). Using intra-vital time-lapse imaging, we compared Tomato^{bright} and Tomato^{dim} BM PCs dynamics in young and middle-aged mice at day 5, day 30 and day 60 post tamoxifen in order to determine the contribution of intrinsic PC age/maturity to their motility and positioning. We could discriminate and track both PC populations on the basis of Tomato expression in the same time-lapse movies (Figure 2C, Supplemental Video S1). At day 5 after treatment, dynamics of both subsets of PCs were similar, based on spider plots, track and displacement velocities, and mean-squared displacement plots (Figure 2D). However, at day 30 and 60 timepoints, Tomato^{bright} PCs showed reduced motility as compared to Tomato^{dim} PCs indicating PC age correlated with reduced cell motility. This effect with PC aging was seen in both young and middle-aged mice, suggesting it was cell intrinsic, and thus related to LLPC maturation. While average speeds for Tomato^{bright} PCs were relatively slow, some rare PCs were highly motile. At day 30 and 60 timepoints, these fast cells were predominantly in Tomato^{dim} populations (Figure 2E), consistent with immature, short-lived PCs having faster motility than LLPCs.

Next we analyzed LLPC spatial organization, as we and others have shown the bulk BM PCs are organized in clusters (Benet et al., 2021; Mokhtari et al., 2015) and that clusters were sites of reduced PC motility (Benet et al., 2021). We used two approaches to determine if LLPCs were more clustered than total Bulk PCs. First, we applied our custom script (Benet et al., 2021)

to identify high density PC clusters. We masked these regions and found that at late timepoints after tamoxifen, Tomato^{bright} LLPCs were more enriched in clusters than bulk PCs (Figure 2F-G). As this approach can be sensitive to PC densities, we developed a second approach to determine if subsets of PCs were enriched in clusters, based on measuring the nearest distance to twenty PC neighbors (Figure 2H). Using this measurement, we found that at day 60, Tomato^{bright} LLPCs were closer to neighboring PCs (i.e., more clustered) than Tomato^{dim} bulk PCs, in the BM of both young and middle-aged mice (Figure 2I). Taken together, while overall PC motility increases with mouse age, most of the increases in motility can be accounted for by bulk PCs and not by LLPCs, which were relatively sessile. This decrease in LLPC motility is also accompanied by an aggregation or retention in PC clusters, suggesting these are LLPC niches, and may be important for their cell-intrinsic survival or retention in the bone marrow.

Differentially expressed surface receptors accompany LLPC maturation

Based on cell intrinsic changes in LLPC motility, we hypothesized that LLPCs may upregulate (or downregulate) unique cell surface receptors as compared to bulk PCs, important for their intrinsic long-term survival and retention in the bone marrow and/or spleen. There are currently no effective surface markers for identifying murine LLPCs and identifying these factors could provide utility for studying LLPCs generation and decay under various vaccination conditions.

Based on existing RNA-seq or microarray datasets (Akhmetzyanova et al., 2021; Cornelis et al., 2020; Lam et al., 2018; Shi et al., 2015), we curated a list of 19 PC markers, which we reasoned might be differentially expressed by LLPCs, based on the high abundance of their gene transcripts in total PCs (Supplemental Figure 2A). To assay their expression, we measured and normalized marker expression (fold-change) on YFP^{+} LLPCs over YFP^{-} bulk PCs, in the bone marrow and spleen of both young and middle-age BEC-YFP mice at day 5, 30, 90 or 150 post

tamoxifen treatment. At day 5, we expected no difference in YFP^+ and YFP^- PCs, an important staining and compensation control for all our replicates.

Overall summary of surface marker expression fold changes for YFP^+ PCs are shown in Figure 3A. As expected, at the early timepoint (D5), there were no differences in the gMFI of all markers between the two populations regardless of the tissue type and age of the mice. However, from day 30 to day 150, 6 out of 19 markers were upregulated (CD93, CD81, CXCR4, and CD326) or downregulated (CD44 and CD48) with PC age (Figure 3B). For the most part, these changes were subtle, whereas CD93 and CD81 expression showed the largest difference in surface expression with PC age (Figure 3C-D). CD93 expression was uniquely bimodal among all tested markers, with YFP^+ LLPCs in BM and spleen were predominantly found in $CD93^+$ subset, in line with genetic evidence for its importance in LLPC maintenance (Chevrier et al., 2009). The cell-intrinsic progressive upregulation of surface CXCR4 level in LLPCs corroborated our previous findings using an adoptive transfer approach (Benet et al., 2021). Other well-known PC factors important for survival were not differentially expressed by LLPCs, such as Syndecan-1 (CD138) (Figure 3E), BCMA (CD269), and TACI (CD267) involved in in APRIL signaling (McCarron et al., 2017) nor CD28 also implicated in PC survival (Utley et al., 2020) (Figure 3A). Some of these LLPC markers (CD44, CD81, CD326 and CD93) showed a larger fold change in young mice as compared to middle-aged mice, in contrast to CXCR4 and CD48 which were not sensitive to mouse age. Splenic LLPCs had higher CD93, CD326 and CXCR4 fold increase over bulk YFP^- splenic PCs, when compared to BM LLPCs fold changes, which may reflect immaturity of YFP^- PCs in the spleen.

Previous characterization of murine LLPCs used glucose uptake, using fluorescent analog, 2NBDG, as a marker for LLPCs (Lam et al., 2018). Indeed, YFP^+ LLPCs had a high (~80%) frequency of 2NBDG in the BM and spleen at day 90 and day 150 post tamoxifen (Supplemental Figure 2B-C). However, while 2NBDG status was different between LLPCs and

bulk PCs in the spleen, there was no differential expression between bulk PCs and LLPCs in the BM, indicating that 2NBDG status may not discriminate between LLPCs and short-lived PCs in the bone marrow.

Previous transmission electron microscopy (TEM) studies have shown changes in morphology during PC maturation (Fooksman et al., 2010; Joyner et al., 2022). We also sorted YFP^+ LLPCs and YFP^- bulk PCs from the spleen and BM at day 90 and conducted TEM to see if morphological differences accompanied LLPC maturation (Supplemental Figure 3). Overall, we did not detect statistically significant differences in cell size, cytoplasmic area, mitochondrial density between mature PC subsets, although the distributions had wide ranges. There were minor yet significant changes in nuclear size and chromatin density in splenic LLPCs over BM LLPCs. Taken together, we conclude that differential surface protein expression accompanies cell-intrinsic LLPC maturation, but otherwise cells appear morphologically similar.

LLPCs accumulate in BM with mouse aging

Using the six differentially expressed surface receptors (Figure 3B), we wondered if this panel of surface markers could be used to reliably identify live murine quasi-LLPCs in WT mice (that lacked BEC-YFP reporter). We validated that the panel was capable of enriching for YFP^+ LLPCs by using the BEC-YFP mice at day 90 post tamoxifen. Ideally, we wanted the minimal panel necessary, thus we analyzed the contribution of different marker(s) alone or combined towards the enrichment of LLPCs, while avoiding any substantial loss of YFP^+ cells. (Supplemental Figure 4). We found that overall, adding more markers increased LLPC enrichment up to 6-fold, in a step-wise, additive manner (Figure 4A and 4B).

While the labeled PCs in BEC-YFP at day 90 or later timepoints are bona-fide LLPCs, they do not represent all of the LLPCs in the tissue, as new LLPCs were generated after time-stamping. Based on changes in PC turnover, PC motility, and surface expression, we hypothesized that

the frequency of LLPCs in the total PC pool of the BM may be increasing with mouse age. Thus, we used our panel to assess the frequency of total LLPCs in WT young and middle-aged mice. Middle-aged mice had a higher frequency of LLPCs in the bone marrow as compared to young mice (Figure 4C), consistent with the decrease in PC turnover (Figure 1G-H). Thus, as mice age, not only do they accumulate more BM PCs (Pioli et al., 2019), but these cells are also more long-lived and mature.

CXCR4 controls durability of humoral responses by promoting PC survival and retention in the BM.

CXCR4 is the master chemokine receptor required for lymphocyte entry and retention in the bone marrow (Zehentmeier and Pereira, 2019). Based on its important role in BM PC motility and retention (Benet et al., 2021), and its upregulated expression on LLPCs (Figure 3B), we decided to test if it is required in PCs specifically to maintain humoral responses. Previous work (Nie et al., 2004) had shown that conditional deletion of *Cxcr4* using a pan B cell expressing cre (CD19-cre) was dispensable for humoral responses and PC survival following vaccination, but potentially this approach did not specifically target PCs and may not be fully penetrant (Aaron and Fooksman, 2022).

To delete *Cxcr4* expression in PCs, we bred BEC *rosa26*^{LSLYFP} *Cxcr4*$^{fl/fl}$ mice (or CXCR4^{cKO}). Cohorts of control BEC-YFP (here referred to as WT) and CXCR4^{cKO} mice were immunized (on day -30) with NP-KLH/Alum to generate similar NP-specific PCs and titers at day -3 (Figure 5A-B, Supplemental Figure 5A-B), at which point, they received tamoxifen to induce *Cxcr4* deletion in CXCR4^{cKO} mice and fate-label PCs with YFP in both groups of mice. We confirmed that *Cxcr4* expression was diminished specifically in YFP^{+} PCs in CXCR4^{cKO} mice at mRNA transcript and protein levels (Figure 5C, Supplemental Figure 5C) at day 60 in the BM and splenic LLPCs but not in control bulk PCs. Interestingly, CXCR4 surface protein levels were significantly reduced but not completely lost, suggesting incomplete deletion in some cells. Nevertheless, anti-NP

titers declined faster in CXCR4^{cKO} mice as compared to WT controls (Figure 5B). Decreases in anti-NP titers were associated with reduced numbers of NP-specific LLPCs (YFP^{+}) in spleen and bone marrow of CXCR4^{cKO} mice as compared to WT mice (Figure 5D).

To determine the role of CXCR4 in homeostatic PC turnover and LLPC competition, we generated chimeric animals using 1:1 ratio of congenically-labeled cells from WT and CXCR4^{cKO} mice. For these studies, mice expressing BEC *rosa26*$^{LSL\text{-}Tomato}$ alleles were used as WT controls. Eight weeks post reconstitution (Figure 5E), mice were treated with tamoxifen and PC decays were tracked over 90 days by flow cytometry. At day 5, fewer PCs were found in the CXCR4^{cKO} vs WT compartment in the bone marrow and spleen (Figure 5F, Supplemental Figure 5D), suggesting labeling efficiency was reduced or there was rapid decline in KO PCs cells from the tissue. Correcting for their relative abundance at day 5, labeled WT (Tomato^{bright}) PCs in BM hardly decayed over 90 days, whereas ~50% of CXCR4^{cKO} were lost (Figure 5G, Supplemental Figure 5E). Within the spleen, PC turnover was overall more rapid, with a 50% and 90% loss of WT and CXCR4^{cKO} labeled PCs, respectively. Overall, WT PCs outcompeted CXCR4^{cKO} PCs in the BM and spleen over time as assessed by competency ratio (Figure 5H, supplemental Figure 5F). We analyzed changes in key PC pro-survival factors, Mcl1 and Bcl2 (Figure 5I-J), and found that WT labeled PCs had higher relative expression than CXCR4^{cKO} counterparts, and while they had similar levels at day 5, PC survival was compromised by loss of CXCR4 over time in bone and spleen suggesting CXCR4 is important for long term survival of PCs.

CXCR4 signaling can directly promote cell survival via AKT pathway (Scotton et al., 2002), but it may act indirectly on PC survival by dislodging from survival niches. Thus, we asked if loss of antigen-specific CXCR4^{cKO} PCs was due to cell death in the bone marrow, or egress from the bone marrow niche, eventually leading to PC loss. Chimeric mice were intra-tibially (IT) injected with 4-hydroxy-tamoxifen (4OH-TAM), to induce cre recombination in PC subsets in one bone (Figure 5K). We used this approach previously to track recirculation of BM PCs (Benet et al.,

2021). At day 1 post injection, WT PCs within the injected tibia were the predominant location of labeled PCs, consistent with a local administration and activity (Figure 5L, Supplemental Figure 5G). However, within CXCR4^{cKO} PC pool, most of the labeled PCs were predominantly found in the spleen, but also found at higher frequencies in other bones. This subset-specific effect is unlikely due to leakage of 4OH-TAM to other tissues, as it would have affected both groups of PCs equally. Thus, the likely conclusion is that CXCR4^{cKO} must have rapidly egressed the BM upon cre-deletion of *Cxcr4*. Over time labeled WT PCs egressed the tibia and redistributed to other sites whereas the labeled CXCR4^{cKO} PC remained fixed in spleen and other niches (Figure 5M). To confirm this effect was due to rapid egress, mice were pretreated with pertussis toxin (PTX), which we had found could block PC motility in the BM (Benet et al., 2021). Pretreatment with PTX prevented CXCR4^{cKO} PCs from accumulating in the spleen, following IT-administration of 4-OH-TAM (Supplemental Figure 5H). Thus, deletion of *Cxcr4* triggers rapid mobilization of PCs from the BM, suggesting dislodging PCs from their niche occurs prior to defects in cell survival.

Shared transcriptional program accompanies BM and splenic LLPC specification

As ASCs mature and migrate to the bone marrow, their transcriptome changes (Shi et al., 2015). Based on the changes in surface expression, we hypothesized that LLPCs may also encode a unique transcriptome that fuel these protein expression differences. Based on previous studies of PC transcriptome studies (Lam et al., 2018), we expected mRNA expression differences in LLPCs to be minor, and due to the over-representation of immunoglobulins in the transcriptome, we performed bulk RNA sequencing with deep reads (50 million reads per sample) to improve our resolution of global changes. For these studies, we FACS-purified matching populations of YFP^{+} LLPCs and YFP^{-} bulk PCs from bone marrow and spleen of BEC-YFP mice, on day 90 post tamoxifen treatment. We used groups from both young and middle-aged mice for these studies to see what effect mouse age played in gene expression or PC composition. As

negative controls, we also sorted YFP^+ and YFP^- PCs from middle-aged mice, on day 5 post treatment. In all, we analyzed 12 groups of PCs (n=3/4 per group, 44 samples total). For these global analyses, we excluded immunoglobulin genes, but analyzed them separately in the next section.

We performed unsupervised clustering of day 90 PC samples using all differentially expressed genes (DEGs) measured by pair-wise comparisons of YFP^+ and YFP^- samples, from matching tissues (p_{adj} <0.05, with no cut-offs for fold-change or reads). Based on the sample dendrogram, we found that most LLPC (yellow) and bulk PC (red) samples clustered separately, and within the LLPCs, BM (light green) and splenic (dark green) samples were closely-related (column headings on Figure 6A). Unsupervised clustering of DEGs (rows) revealed five groups of genes (Figure 6A, Supplemental Table 1). Specifically, groups 5 and 2 genes contained DEGs that were either upregulated or downregulated in all LLPC groups, respectively. Group 1 genes were specifically upregulated in splenic LLPCs, suggesting tissue-specific expression patterns. To better understand the overlaps or similarities of these LLPC groups, we generated an UpSet analysis plot (Conway et al., 2017; Lex et al., 2014), based on pair-wise comparisons (Figure 6B). Splenic LLPCs from young and middle-aged mice had the most DEGs, likely because splenic (YFP^-) bulk PCs used in comparisons were highly enriched in short-lived PCs. Among DEGs shared among LLPC subsets, many were shared by 3 or 4 of groups. 12 DEGs were shared by all LLPCs (*Cd55*, *Cxcr3*, *Cyp4f18*, *Fam3c*, *Gpx3*, *H2-Aa*, *H2-Ab1*, *Hcst*, *Prss57*, *Rab3b*, *Slamf6*, *Spag5*). As negative controls, comparisons of day 5 YFP^+ vs YFP^- PCs were conducted, and as expected, very few DEGs were detected or shared with LLPCs. Using circle plots (Figure 6C), we summarized the overlaps of DEGs, and found that BM LLPCs DEGs were more commonly shared among LLPC groups, as compared to splenic LLPCs. We also observed that LLPCs from middle-aged mice had fewer DEGs than young mice, consistent with the view that bulk PCs (YFP^-) are enriched with LLPCs in older mice (Figure 4C).

Next, to determine which biological pathways were altered in LLPCs, we generated GO-terms based on the previously identified DEGs, and assessed term-enrichment in LLPC subsets and day 5 control groups (Figure 6D). As expected, LLPCs showed downregulation of MHC Class II pathway and proliferation related pathways. In contrast, LLPCs showed increased in cell survival and stress response pathways, increased lipid metabolism, and neural-immune signaling. Changes in cell adhesion and chemotaxis were highly enriched in LLPCs and there were also changes in cytokine production pathways. From the total DEG list, putative cell surface receptors were extracted to generate heatmaps of normalized expression among PC subsets in the BM and spleen, clustered by DEG groups (Figure 6E). These included chemokine receptors (*Ccr10*, *Cxcr3*, *Ccr9*, *S1pr1*, *Ebi3*), adhesion molecules (L-selectin, *Ly6* family, Galectins, *Cd93*), MHC-related molecules, co-stimulatory factors (SLAM family, *Tigit*), and cytokine receptors (*Il6st*, *Il13ra1*, *Ifnar2*, *Tgfb2*) to name a few. Some of these LLPC factors were tissue-specific, such as *C1q* and *Adgre5* expressed by splenic LLPCs. There were notable absences from the list, such as *Cxcr4*, which is upregulated at the protein level in LLPCs, suggesting that minor changes in transcripts may be regulating larger changes at the protein level, or important regulation may be occurring post-transcriptionally (Greenbaum et al., 2003).

We also generated a putative list of transcription factors (TF) and chromatin-remodeling factors differentially expressed in LLPCs (Figure 6F). Among known PC-related factors, *Bmi1* (Di Pietro et al., 2022) was upregulated in LLPCs while *Myb* (Good-Jacobson et al., 2015), *Klf2 (Winkelmann et al., 2011)* and *Zbtb32* (Jash et al., 2019) were down-regulated. Interestingly, *Aire* (Mathis and Benoist, 2009) was among the most upregulated LLPC genes, but its role in PCs has not been explored. Many classical PC TFs were not differentially expressed by LLPCs, including *Prdm1* (encoding Blimp1), *Irf4*, and *Xbp1*. Taken together, murine LLPCs exhibit a

unique global transcriptome, fine-tuning surface receptors and transcriptional factor expression, which may support longevity.

LLPC receptors have reduced BCR diversity but enriched in public clones.

As expected, the major RNA transcript in these PCs were immunoglobulin heavy and light chains. We assembled over 26,000 complete clones (but not paired sequences) for the BCR heavy and light loci and analyzed their clonal properties, to determine if LLPCs had unique features in different tissues and are from mice of different ages. Notably, these are unselected polyclonal PCs from naïve mice, with unknown antigen specificities.

First, we analyzed isotype usage and found that IgA PCs were the major isotype within the BM and also in the spleen, to a lesser extent (Figure 7A). The one notable exception was that splenic LLPCs from young mice that were time-stamped at 6-8 weeks of age were highly enriched in IgM, in comparison to all other samples, including splenic bulk PCs from same (young) mice. This suggest that these splenic IgM LLPCs are specified early in life and tend to be selectively retained, and maybe derived from B-1 lineages (Baumgarth, 2016). Within LLPCs subsets, both in young and middle-aged mice, BM LLPCs have a higher IgA:IgM composition as compared to splenic LLPC counterparts, suggesting tissue-specific homing or retention of different LLPCs on the basis of isotype.

Next, we analyzed diversity of clones in the LLPC and bulk PC subsets, by comparing the heavy chain V-segment + CDR3 exact amino acid sequences. We found that LLPC samples (day 90 YFP^+ BM and spleen) had reduced clonal diversity based on Chao1 estimation index (Figure 7B) as compared to bulk (day 90 YFP^- BM and spleen) PCs, while no differences were observed between YFP^+ and YFP^- subsets at day 5 post TAM. This suggested LLPCs had a reduced repertoire and complexity compared to bulk PCs. This also raised the possibility that different subsets of clones were selected for LLPC fate specification.

Based on the isotype differences and reduced diversity in LLPCs compared to bulk PCs, we calculated frequencies of shared clones from different PC groups within the same mouse (Figure 7C), in order to see if LLPC and bulk PCs arise from same pool of B cells. We also analyzed if PCs from BM and spleen had shared clones, to see if related clones can home to either sites migrate to both sites or possibly recirculate (Benet et al., 2021). As controls, PCs from day 5-treated mice showed the highest overlap of clones between YFP^+ and YFP^- subsets in all tissues, along with bulk (YFP^-) PCs in BM and spleen, consistent with their heterogenous PC phenotypes and coordinated timing for PC differentiation. LLPCs in the BM and spleen shared more clones in common amongst themselves than with bulk PCs in the same tissue or other sites. This is consistent with either a PC repertoire changing over time with mouse age or unique selection of certain clones into LLPC fate base on specificity. This trend was more striking in young mice, which have fewer LLPCs in the YFP^- subset than in middle-aged mice, suggesting these LLPCs may arise from a different population of B cells in young mice.

LLPCs have been suggested to arise from germinal centers, which could suggest that residency time in the GC may regulate selection into the LLPC pool. To see if polyclonal LLPCs were more highly mutated than total bulk PCs, we compared overall somatic hypermutation (SHM) frequencies in V regions matching samples of YFP^+ (LLPC) and YFP^- (bulk PCs) and found that day 90 LLPC clones had fewer mutations than bulk PCs in BM or spleen whereas no differences in mutations were observed between day 5 samples (Figure 7D). When averaging all clones per sample, LLPCs also had fewer SHM than paired bulk PC samples in the same tissue of the same mouse. (Figure 7E). LLPCs timestamped at 6-8 weeks (young mice) had even fewer mutations than LLPCs in middle-aged mice. Overall, this confirms that PC cells need not arise from affinity-selected GC B cells in order to enter the LLPC pool.

Finally, to see if certain clones were “public” (or shared by at least 2 samples from different mice), we analyzed heavy chain clonal overlap (as in Figure 7B-C) in all samples. Young mice

had the highest overlap of shared public clones compared to other groups (Figure 7F). We analyzed which groups of PCs were responsible for this elevation and found that LLPCs in BM and spleen accounted for most of the public clones (Supplemental Figure 6A). Next, we analyzed the top 100 most abundant public clones across all samples (Supplemental Figure 6B) and found a biased enrichment towards LLPC samples (Figure 7G). While LLPCs represented about 28% of all found clones (n= 26144), in the top public clones across samples, 75% were found in LLPC samples from multiple tissues and mice (Figure 7H). Among the top LLPC public clones (found in >75% of LLPC samples, Supplemental Figure 6B), they were surprisingly absent in bulk PC groups (Figure 7I). This suggests that the some of LLPC endogenous repertoire is directly selected into the LLPC compartment for long term maintenance.

DISCUSSION

The mechanisms and conditions underlying cell fate into long-lived plasma cells following vaccination remains a long-standing question for durable humoral memory. Moreover, once LLPCs are specified, the intrinsic programming and extrinsic factors that control their longevity are still undefined (Robinson et al., 2022; Robinson et al., 2020). While the field has leaned towards a model that LLPCs arise from late GC B cells (Weisel et al., 2016), LLPCs can be generated by T-independent fashion (Bortnick et al., 2012) as well. Recent work using similar PC time-stamping tools have demonstrated that NP-specific LLPCs can arise from pre-GC stages and accumulate at constant click during the immune response, showing no bias towards late stages (Robinson et al., 2022) nor requiring high affinity for longevity, at least in the NP-immunization model. In “naïve” mice, which are not biased by immunization, we find clones selected into LLPCs pool bear fewer somatic mutations than bulk PCs, consistent with recent

scRNA-seq analysis (Liu et al., 2022), and aforementioned findings that LLPC generation is not strictly dependent on late GC B cells following immunization (Robinson et al., 2022) (Koike et al., 2023). We also find limited diversity in BCR repertoire, which may reflect unique clones or antigens are pre-programmed for LLPC or, merely that longer immune responses engender more clonal LLPC over time (Robinson et al., 2022). We also find LLPCs are enriched in public or shared clones, which have been recently shown to be microbial and self-reactive (Blanc et al., 2016; Lino et al., 2018; Liu et al., 2022; Racine et al., 2011). Interestingly, while some of our public clone lists have shared V-regions with known self-reactive and microbial specificities, many are not found on any of these lists, suggesting variations in microbiome composition or diet may shift the LLPC clonal composition.

We also find differences in the isotype compositions of endogenous LLPCs in naïve mice based on tissue and mouse age. Within the BM, we found that IgA^+ LLPCs are the major subset, similar to the bulk BM PC composition, in line with previous studies (Liu et al., 2022; Xu et al., 2020), and likely depend on microbial composition in the gut (Liu et al., 2022; Wilmore et al., 2018). In contrast, the majority of splenic LLPCs are a mix of IgM^+ and IgA^+ LLPCs, and particularly in young mice, IgM^+ LLPCs seem to be preferentially generated and retained in the splenic niche. While IgM^+ LLPCs can be generated by various pathways, including infection or immunizations (Blanc et al., 2016; Racine et al., 2011), and even persist in germ-free mice (Lino et al., 2018), this early wave of IgM^+ LLPCs is consistent with B-1-derived precursors that maintain natural antibodies in the spleen and peritoneal cavity (Baumgarth, 2011, 2016). Indeed, we find that LLPCs timestamped early (in young mice) had more public clones, less diversity and limited SHM, which may further indicate these cells are derived from B-1 lineage (Vergani et al., 2022). Recent time-stamping work has pointed out that IgM isotypes have longer half-lives than IgG PCs and IgA (Koike et al., 2023) (Liu et al., 2022), suggesting unique transcriptional programs that may preferentially retain these IgM LLPCs in PC niches through

668 altered adhesion receptor expression (Higgins et al., 2022; Liu et al., 2022), at the cost of newly
669 minted PCs, presumably from B-2-derived responses. LLPC clones are shared across the BM
670 and splenic compartment, suggesting these niches can be redundant and may accommodate
671 LLPC recirculation between sites (Benet et al., 2021).

672 We find unique transcriptome and proteome expressed by endogenous LLPCs that underlie
673 their intrinsic longevity. On the RNA level, these changes are minor, as others have noted (Lam
674 et al., 2018), and often below detection limits for standard fold-change cut-offs or heterogeneity
675 in the LLPC pool (Liu et al., 2022). However, these small changes can reflect larger changes in
676 protein levels, particularly within cells that are optimized for massive protein production,
677 suggesting that proteomics may be a more appropriate way to study changes in PC to LLPC
678 maturation changes. Among the GO-terms and DEGs found, most are shared by LLPCs in the
679 BM or spleen suggesting similar requirements for survival or that these cells are recirculating
680 between niches over time, consistent with clonal overlap between both sites (Figure 7C), and in
681 line with what we have reported for bulk PCs (Benet et al., 2021). However, we find that cluster
682 1 of DEGs among splenic LLPCs, associated with IgM-specific factors such as complement
683 receptors, in line with recent study (Higgins et al., 2022) indicating that IgM^+ LLPCs have unique
684 expression and potentially functional roles in the spleen (Bohannon et al., 2016). In contrast,
685 we did not find major changes in metabolism based on GO-terms, glucose uptake,
686 mitochondrial density, suggesting PC function and longevity are not directly linked. Many of the
687 LLPC DEGs were surface proteins, suggesting cell dynamics, and cell communication changes
688 are critical for LLPC function and longevity.

689 A major goal of our study was to address what changes LLPCs have adapted to maintain their
690 survival while most PCs are short-lived. Mechanistically, are their lifetime intrinsically-regulated
691 by an internal clock (Robinson et al., 2022) as with GC B cells (Mayer et al., 2017), or by
692 competition with other PCs for a limited niche? Our imaging data supports the later model as

693 part of that process. We find that LLPCs are preferentially arrested and clustered in the bone
694 marrow in a cell intrinsic manner. This paucity in LLPC movement stands in contrast to the
695 intermittent burst speeds of the neighboring bulk PCs, enriched in short-lived PCs, highlighting
696 that change in motility is a cell-intrinsic program rather than merely stochastic or spatially
697 controlled by certain extrinsic cues, as suggested in T cells (Fowell and Kim, 2021). Indeed,
698 both LLPCs and bulk PCs can be observed residing in one cluster, suggesting all PCs can
699 share and potentially compete for the same cell-extrinsic cues, however the proportion and
700 lifetime of LLPCs within these complexes is higher and longer, suggesting residency is
701 important. We do observe LLPCs displaced from these structures suggesting that competition
702 may be dynamic process. Indeed, transfer of PCs into B cell-deficient mice have longer
703 lifetimes than seen in immunocompetent mice, suggesting PC survival is competitive (Bohannon
704 et al., 2016). Moreover, rapid depletion of BM PCs using CD138-DTR mouse leads to rapid
705 recovery of BM PCs at a similar density as before (Koike et al., 2023), suggesting a limited
706 niche size (Sze et al., 2000).

707 What factors underlie LLPC clustering? We previously showed that hematopoietic-derived
708 APRIL promotes BM PC clustering and motility, suggesting it may be enriched in clusters (Benet
709 et al., 2021). However, receptors for APRIL, TACI and BCMA, and co-receptor CD138, were
710 not differentially expressed on LLPCs, suggesting enhanced ligand-receptor binding is unlikely
711 to play an important role in LLPC retention in the niches, or directly leading to enhanced LLPC
712 survival. Potentially, the upregulation of adhesion molecule such CD93 (Chevrier et al., 2009)
713 and CD326 (EpCAM) (Gires et al., 2020) may help LLPCs dock the niches for a prolonged
714 period of time and hence longer survival, along with the other changes we detected in our
715 surface expression profiling, including multiple changes in SLAM and *Ly6* family protein
716 expression. Thus, their longevity fate may be shaped by multiple cell-intrinsic homing and
717 retention factors that promote preferential docking at these sites. These cell-intrinsic changes in

motility and positioning that accompany LLPC specification are likely critical to their long-term maintenance over newly minted PCs.

Among these differentially expressed homing factors, we have been particularly focused on CXCR4's functional role in BM PC motility and LLPC survival. We have found that LLPCs upregulate CXCR4 over other PCs, and PC-intrinsic deletion of CXCR4 led to rapid egress from the BM, leading to reduced overall PC survival, disrupting NP-specific antibody titers. Our model directly targets CXCR4 during the PC stage, in an inducible fashion, in contrast with a previous study (Nie et al., 2004) that used a constitutive deletion of CXCR4 in B cell lineage and found no effect on humoral immunity. CXCR4 plays multiple roles through B cell differentiation, including during the germinal center (Allen et al., 2004), thus early deletion of CXCR4 may result in compensatory mechanisms in their model. While it is tempting to simply conclude that increased CXCR4 expression by LLPCs directly leads to cell-intrinsic arrest in BM niches, we have also showed that CXCR4 promotes BM PC motility, and inhibitors quickly perturb PC motility (Benet et al., 2021). One possibility could be dynamics in chemokine receptor expression or ligand availability may be at play. While CXCL12 is ubiquitously expressed within the BM (Benet et al., 2021), lower levels of CXCL12 in some regions of parenchyma or reduced CXCR4 expression may foster cell movement or chemokinesis, whereas higher CXCR4 levels on LLPCs may promote cell-intrinsic arrest in CXCL12-rich niches (Lammermann and Kastenmuller, 2019). Moreover, gain-of-function alleles of CXCR4 also lead to shortened humoral responses, while increasing the number of total PCs (Biajoux et al., 2016), which further suggests that a dynamic range in CXCR4 signaling within PC pool is important for regulating LLPC survival, in a competitive manner (Aaron and Fooksman, 2022). Thus, CXCR4 may coordinate with other spatial positioning factors to give LLPCs optimal positioning in limited niches (Hauser et al., 2002; Lammermann and Kastenmuller, 2019).

As mice age, PCs accumulate in the bone marrow (Pioli et al., 2019) and other sites (Nunez et al., 2016; Schaum et al., 2020), but we now report that this increase is accompanied by an enrichment in LLPCs within the PC pool based on surface marker expression and by reduced turnover of BM PCs in middle-aged mice. Increases in LLPCs presumably raises the threshold needed for newly generated PCs to be retained and survive in the BM. By intravital imaging, we see that overall PC speeds increase in older mice (Benet et al., 2021), which is likely due to faster motility by short-lived PCs, as LLPCs remain largely sessile. These faster and longer movements may reflect that short-lived PCs are unable to find open survival niches. This indicates that PC niches in the BM are limited, and may be sites of competition between newly-minted PCs and LLPCs. Indeed, as mice age, increases in pre-existing LLPCs may further limit the survival capacity of newly-minted PC leading to weakened and shortened serological responses. Thus, in improving weak and short-lived humoral responses in older adults (Fedele et al., 2022; Wagner and Weinberger, 2020)., we may need to consider the role of LLPCs competition in regulating these processes.

AKNOWLEDGMENTS

We would like to thank Dr. Yongwei Zhang, Einstein Transgenic facility, for helping construct BEC mice, Dr. Xusheng Zheng for help with generating surface marker heat map, Einstein Flow cytometry core for FACS sorting, Einstein Genomics Core for bioanalysis, Einstein Analytical Imaging Facility for help with EM imaging and analysis. This work was supported by R01HL141491 (DRF), Irma T. Hirschl/Monique Weill-Caulier Trusts Research Award (DRF), R01AI132633 (KC) with support from the Albert Einstein NCI Cancer Center grant P30CA013330., SIG #1S10OD016214-01A1. We thank Leslie Cummins for help analyzing and preparing EM images. We thank Dr. Gregoire Lauvau for comments on the manuscript.

AUTHOR CONTRIBUTIONS

The study was conceived, designed, by D.R.F. and Z.J, who also wrote the manuscript. Z.J. conducted experiments for all figures. L.O. contributed to Figure 4. R.P. contributed work that supported conclusions in Figure 2. S.W. analyzed EM data in Supplemental Figure 3. K.C. and M.D. generated unique reagents. P.G., D.Z. analyzed global RNAseq transcriptome Figure 6, and T.M. helped with BCR clonal analysis for Figure 7. Y.H. developed nearest-neighbor analysis for Figure 2.

774

FIGURE LEGENDS

Figure 1. Plasma cell turnover rate decreases with mouse age.

(A), PC purity of TdTomato^{+}YFP^{-} and TdTomato^{+}YFP^{+} cells in BEC-YFP mouse at day 5 post tamoxifen treatment. (B), Percentage of YFP^{+} PCs in BEC-YFP mouse in the absence of tamoxifen treatment or treated for 3 consecutive days and analyzed 5 days after the last treatment. (C), Experimental setup for measuring homeostatic PC turnover rate in young and middle-aged mice by timestamping at day 5, 30, 90, and 150 after oral gavage tamoxifen treatment, accompanied by transcriptional profiling using bulk RNA-seq at day 5 and 90 and morphological characterization using transmission electron microscopy at day 90. (D), FACS pseudo color plots showing decay kinetics of percentage of TdTomato^{+}YFP^{+} in total B220^{-} TdTomato^{+} PCs remaining in the BM (upper panel) and spleen (lower panel) in young and middle-aged mice, quantified in (E) for BM and (F) for spleen. (G) and (H), Absolute numbers (left panel) and half-lives ($t_{1/2}$) (right panel) of TdTomato^{+}YFP^{+} PCs in the BM (H) and spleen (I) in young and middle-aged mice. Curve fitting and $t_{1/2}$ calculations were conducted by using absolute numbers fitted in a one-phase decay model. All bars show mean (E-H) or mean ± SD (D and I). *, P< 0.05; **, P< 0.01; ****, P< 0.0001; ns, non-significant by unpaired Student's t test. All graphs show pooled data from at least two independent experiments. (E, n = 6-18; F, n = 7-13; G, n = 6-21; H, n = 7-13)

Figure 2. BM LLPCs display cell-intrinsic arrest and clustering.

(A), Experimental setup for intratibial two-photon intravital imaging of both TdTomato^{dim}YFP^{+} bulk PCs and TdTomato^{bright}YFP^{+} LLPCs in the same young or middle-aged mouse by timestamping at day 5, 30, and 60 after oral gavage tamoxifen treatment. (B), FACS gating strategy (left panel) for TdTomato^{dim}YFP^{+} bulk PCs and TdTomato^{bright}YFP^{+} LLPCs after intravital imaging and surface CXCR4 and CD93 expression (right panel) on TdTomato^{dim}YFP^{+} bulk PCs

compared to TdTomato^{bright}YFP^{+} LLPCs at day 5 (control timepoint) and day 60 post tamoxifen treatment. (C), Time-lapse images highlighting the cell migration trajectories of 4 bulk PCs (green spot with light purple tracks) and 2 LLPCs (yellow spots with red tracks) in a small region of BM parenchyma. Scale bars, 7 μm. (D), Individual cell tracks of total bulk PCs or LLPCs plotted at a common origin (left panel) in young and middle-aged mice at day 5, 30, and 60 post tamoxifen treatment. Comparison of total bulk PCs and LLPCs track velocity (middle left panel), track displacement velocity (middle right panel), and mean-squared displacement (right panel) in young and middle-aged mice at day 5, 30, and 60 post tamoxifen treatment. (E), Fractions of fast-moving cells (track velocity > 1 μm/min) in bulk PCs compared to LLPCs at day 30 and 60 post tamoxifen treatment. Data were pooled from young and middle-aged mice for each timepoint. (F) Representative intravital 3D flattened image of masked intensity channels of bulk PCs (green) and LLPCs (yellow) (upper panel) and PC spots (bulk PCs in green and LLPCs in yellow) and cluster surfaces (purple) (lower panel) identified for analysis in (G). (G), Average percentage of bulk PCs compared to LLPCs staying inside cluster surface over time (left panel). Average time of individual bulk PCs spent inside cluster surface compared to that of LLPCs (right panel). (H) Depiction of nearest neighbor analysis for cell-cell distance (lines) in 3D (collapsed in 2D) between bulk PCs (green) and total PCs (green and orange), or between LLPCs (orange) and total PCs (green and orange), which is quantified in (I) for an average distance between bulk PCs or LLPCs and their 20 nearest neighbor cells (total PCs combining bulk PCs and LLPCs). Each symbol represents one randomly picked cell per subset, and data were pooled from at least two mice. All bars show mean (F, G, H, and I) or mean ± SEM (D and G). *, P< 0.05; **, P< 0.01; ****, P< 0.0001; exact p-values; ns, non-significant by Mann Whitney U test (D), Kruskal-Wallis test with Dunn's test for multiple comparisons (I), or paired Student's t test (E and G). All graphs show pooled data from at least two independent experiments. (E, n = 3-5; I, n = 4)

Figure 3. Differentially expressed surface receptors accompany LLPC maturation.

(A), Heatmap depicting average fold changes of surface marker expression level (gMFI) on TdTomato^{+}YFP^{+} LLPCs and TdTomato^{+}YFP^{-} bulk PCs from 3-4 mice per unit at indicated timepoints post tamoxifen treatment in the bone marrow and spleen of young and middle-aged mice. Color scale showing fold increase in red, fold decrease in blue, or no difference in white. (B), Overlay histograms comparing the expression level of differentially expressed surface markers on TdTomato^{+}YFP^{-} bulk PCs to TdTomato^{+}YFP^{+} LLPCs at day 90 post tamoxifen treatment. (C-E), The fold change of the expression level (gMFI) of differentially expressed surface markers (CD93 (C), CD81 (D), CD138 (E)) on TdTomato^{+}YFP^{+} LLPCs relative to TdTomato^{+}YFP^{-} bulk PCs in individual mouse at indicated timepoints post tamoxifen treatment in the bone marrow (upper panel) and spleen (lower panel) of young and middle-aged mice. All bars show mean ± SEM (C-E). *, P< 0.05; **, P< 0.01; ***, P< 0.001; ****, P< 0.0001; ns, non-significant by unpaired Student's t test. All graphs show pooled data from at least two independent experiments. (A,C-E, n = 3-7)

Figure 4. LLPCs accumulate in the BM with mouse aging.

(A), Percentage of TdTomato^{+}YFP^{+} LLPCs after enrichment using a combination of 1-6 antibody panel of differentially expressed surface markers identified in Figure 3. 0 marker represents the percentage of TdTomato^{+}YFP^{+} LLPCs at day 90 post tamoxifen in young mice. (B), Representative FACS contour plots showing the fractions of YFP^{+} LLPCs in total TdTomato^{+} PCs after enrichment using a combination of 1-6 antibody panel of differentially expressed surface markers. (C), Percentage of quasi-LLPCs in total PCs identified using 6-marker antibody panel in young and middle-aged mice at steady state. All bars show mean (C). **, P< 0.01, by unpaired Student's t test. All graphs show representative data of at least two independent experiments. (C, n = 5-6 mice)

Figure 5. CXCR4 controls durable humoral response by promoting PC survival and retention in the BM.

(A), Experimental set up for examining the role of CXCR4 in sustaining antigen-specific antibody responses using a NP-KLH/Alum immunization model. i.p., intraperitoneal. (B), Anti-NP antibody titer in WT or CXCR4^{cKO} mice before tamoxifen treatment at day 30 post immunization (left panel) and the remaining percentage of pre-treat anti-NP antibody at indicated timepoints post tamoxifen treatment (right panel). (C), Fold change of FACS-purified YFP^{+} PCs *Cxcr4* mRNA level in WT or CXCR4^{cKO} mice, normalized to *Actb* levels in WT mice. (D), Absolute numbers of NP-specific bulk PCs and LLPCs in the bone marrow (left panel) and spleen (right panel) of WT and CXCR4^{cKO} mice. (E), Experimental set up for generating mixed bone marrow chimera reconstituted with WT and CXCR4^{cKO} donors. (F), Absolute number of (YFP^{+}) labeled BM and spleen PCs at indicated timepoints post tamoxifen treatment (G) normalized labeled PC numbers shown in (F) (relative to day 5 post tamoxifen treatment). (H) PC competitive competency (right panel) at indicated timepoints determined by normalizing the CXCR4^{cKO}:WT ratio in the bone marrow labeled PC compartment to that of total splenic B cell compartment (upper panels) or the CXCR4^{cKO}:WT ratio in the splenic labeled PC compartment to that of total splenic B cell compartment (lower panels). (I and J), Mcl1 (I) and Bcl2 (J) intracytoplasmic expression (by gMFI) of WT or CXCR4^{cKO} labeled PC compartment at indicated timepoints in the bone marrow (left panel) and spleen (right panel). Fold changes of WT over CXCR4^{cKO} labeled PCs in Mcl1 and Bcl2 expression level are indicated above the statistical significance symbol. (K), Experimental set up for intratibial injection into WT:CXCR4^{cKO} mixed bone marrow chimera in the presence or absence of pertussis toxin treatment. (L), Absolute number of labeled WT or CXCR4^{cKO} PC in injected tibia and distal organs/tissues at day 1 post 4-OH-TAM injection. (M), Distribution of absolute numbers of labeled WT or CXCR4^{cKO} PCs in injected tibia and distal organs/tissues. All bars show mean ± SEM. Each symbol in all plots represents one

mouse. *, P< 0.05; **, P< 0.01; ***, P< 0.001; ****, P< 0.0001; ns, non-significant by unpaired Student's t test (B, C, D, F-G, L, and M), paired Student's t test (I and J) or one-way ANOVA with multiple comparison correction using the Holm-Šídák test (H). All graphs show pooled data from two independent experiments. (B, n = 13-15 (left), n = 6-9 (right); C, n = 4-8; D, n = 6-9; F-H, n = 8-10; I, n = 8-10; J, n = 8-10; L-M, n = 4)

Figure 6. Shared transcriptional program accompanies BM and splenic LLPC specification

(A), Heatmap depicting unsupervised clustering of total differentially expressed genes (DEGs, p_{adj}-value < 0.05) between TdTomato^{+}YFP^{-} bulk PCs to TdTomato^{+}YFP^{+} LLPCs across tissue types (bone marrow and spleen) and mouse ages (young and middle-aged) at day 90 post tamoxifen treatment, with no cutoff for fold change and transcripts per million reads (TPM). Color scale represents z-score for normalization per gene (row). Total DEGs were separated in 5 color-coded clusters. (B), UpSet plot visualizing total number of DEGs in each pair-wise comparison (single node) and intersections (connecting nodes) between DEGs among different pair-wise comparisons. (C), Pie charts showing the fractions of the DEGs that are unique in one pair-wise comparison group or shared by 2-4 groups of pair-wise comparisons. Numbers in the center of each chart represents the total number of DEGs in each indicated pair-wise comparison group. (D), Bubble plots showing selected gene ontology terms (GO terms) enrichment comparing LLPCs groups (highlighted in yellow) and day 5 control groups bulk PCs (highlighted in red) based on previously identified DEGs in (A). Color scale bar showing the percentage of DEGs upregulated per GO term in each pair-wise comparison group (red, > 50% upregulated DEGs; blue, < 50% upregulated DEGs). Circle size represents the significance of the enrichment based on the -log10(p-value). (E and F), Heatmap of all DEGs encoding surface proteins (E) or transcription factors (F) between LLPC groups and bulk PC groups in both the

spleen (left) and the bone marrow (right), which are further separated by gene clusters identified in (A).

Figure 7. LLPC receptors have reduced BCR diversity but enriched in public clones.

(A), Stacked bar plots showing isotype gene usage (the fraction of isotypes in total mapped complete clones per group) in LLPCs and bulk PCs at day 5 and 90 post tamoxifen treatment across tissue types (spleen and bone marrow) and mouse ages (young and middle-aged). Line thickness represents the statistical significance based on p-value thresholds. Line color represents the comparisons of color-coded isotypes between groups. (B), BCR repertoire diversity of LLPCs and bulk PCs at indicated timepoints across tissue types (spleen and bone marrow) and mouse ages (young and middle-aged), estimated by chao 1 richness index for the abundance of unique clones in a repertoire per group. Each symbol represents one mouse, and pooled bulk PC samples comparing pooled LLPC samples at day 90 post tamoxifen treatment were shown on the right in black. (C), The percentage of clones shared by indicated PC subsets within the same mouse (intra-mouse). X axis format (A::B) reflects samples A & B used for comparison. (D), Violin plots comparing the distribution of somatic mutation frequencies per specific V region (across all clones) in YFP^- bulk PCs and YFP^+ LLPCs at indicated timepoints in young and middle-aged mice. Each symbol represents one clone, and multiple samples were pooled from each group. (E), Average mutation frequencies of all clones in (D) for each PC subset in indicated tissues in young and middle-aged mice. Each symbol represents one mouse. (F), The percentage of clones shared by all samples, day 5 samples, middle-aged mice samples, and young samples. Each symbol represents one sample (e.g., BM YFP^+ sample, BM YFP^- sample, etc.). (G), Frequency of top 100 most abundant public clones in all PC samples compared to that in LLPC samples. Clones showing no preference for LLPC samples over total samples are distributed on the diagonal line in the plot. Each symbol represents a clone. (H), Pie charts showing the fraction of total clones or top 100 most abundant public clones in LLPCs

compared to other PCs. (I), Stacked bar plots showing the distribution of sample types (in tissues and age of mice) per most frequent public clone in LLPCs. Number on the right of each stacked bar represents the number of mice. *, P< 0.05; **, P< 0.01; ****, P< 0.0001; exact p-values for non-significance by unpaired Student's t test.

References

Aaron, T.S., and Fooksman, D.R. (2022). Dynamic organization of the bone marrow plasma cell niche. FEBS J *289*, 4228-4239.

Akhmetzyanova, I., Aaron, T., Galbo, P., Tikhonova, A., Dolgalev, I., Tanaka, M., Aifantis, I., Zheng, D., Zang, X., and Fooksman, D. (2021). Tissue-resident macrophages promote early dissemination of multiple myeloma via IL-6 and TNFalpha. Blood Adv *5*, 3592-3608.

Allen, C.D., Ansel, K.M., Low, C., Lesley, R., Tamamura, H., Fujii, N., and Cyster, J.G. (2004). Germinal center dark and light zone organization is mediated by CXCR4 and CXCR5. Nature immunology *5*, 943-952.

Baumgarth, N. (2011). The double life of a B-1 cell: self-reactivity selects for protective effector functions. Nat Rev Immunol *11*, 34-46.

Baumgarth, N. (2016). B-1 Cell Heterogeneity and the Regulation of Natural and Antigen-Induced IgM Production. Front Immunol *7*, 324.

Benet, Z., Jing, Z., and Fooksman, D.R. (2021). Plasma cell dynamics in the bone marrow niche. Cell reports *34*, 108733.

Biajoux, V., Natt, J., Freitas, C., Alouche, N., Sacquin, A., Hemon, P., Gaudin, F., Fazilleau, N., Espeli, M., and Balabanian, K. (2016). Efficient Plasma Cell Differentiation and Trafficking Require Cxcr4 Desensitization. Cell reports *17*, 193-205.

Blanc, P., Moro-Sibilot, L., Barthly, L., Jagot, F., This, S., de Bernard, S., Buffat, L., Dussurgey, S., Colisson, R., Hobeika, E., *et al.* (2016). Mature IgM-expressing plasma cells sense antigen and develop competence for cytokine production upon antigenic challenge. Nat Commun *7*, 13600.

Bohannon, C., Powers, R., Satyabhama, L., Cui, A., Tipton, C., Michaeli, M., Skountzou, I., Mittler, R.S., Kleinstein, S.H., Mehr, R., *et al.* (2016). Long-lived antigen-induced IgM plasma cells demonstrate somatic mutations and contribute to long-term protection. Nat Commun *7*, 11826.

Bolotin, D.A., Poslavsky, S., Mitrophanov, I., Shugay, M., Mamedov, I.Z., Putintseva, E.V., and Chudakov, D.M. (2015). MiXCR: software for comprehensive adaptive immunity profiling. Nature methods *12*, 380-381.

Bortnick, A., and Allman, D. (2013). What is and what should always have been: long-lived plasma cells induced by T cell-independent antigens. J Immunol *190*, 5913-5918.

Bortnick, A., Chernova, I., Quinn, W.J., 3rd, Mugnier, M., Cancro, M.P., and Allman, D. (2012). Long-lived bone marrow plasma cells are induced early in response to T cell-independent or T cell-dependent antigens. J Immunol *188*, 5389-5396.

Chevrier, S., Genton, C., Kallies, A., Karnowski, A., Otten, L.A., Malissen, B., Malissen, M., Botto, M., Corcoran, L.M., Nutt, S.L., and Acha-Orbea, H. (2009). CD93 is required for maintenance of antibody secretion and persistence of plasma cells in the bone marrow niche. Proc Natl Acad Sci U S A *106*, 3895-3900.

Conway, J.R., Lex, A., and Gehlenborg, N. (2017). UpSetR: an R package for the visualization of intersecting sets and their properties. Bioinformatics *33*, 2938-2940.

Cornelis, R., Hahne, S., Taddeo, A., Petkau, G., Malko, D., Durek, P., Thiem, M., Heiberger, L., Peter, L., Mohr, E.*, et al.* (2020). Stromal Cell-Contact Dependent PI3K and APRIL Induced NF-kappaB Signaling Prevent Mitochondrial- and ER Stress Induced Death of Memory Plasma Cells. Cell Rep *32*, 107982.

Di Pietro, A., Polmear, J., Cooper, L., Damelang, T., Hussain, T., Hailes, L., O'Donnell, K., Udupa, V., Mi, T., Preston, S.*, et al.* (2022). Targeting BMI-1 in B cells restores effective humoral immune responses and controls chronic viral infection. Nature immunology *23*, 86-98.

Dobin, A., Davis, C.A., Schlesinger, F., Drenkow, J., Zaleski, C., Jha, S., Batut, P., Chaisson, M., and Gingeras, T.R. (2013). STAR: ultrafast universal RNA-seq aligner. Bioinformatics *29*, 15-21.

Fedele, G., Trentini, F., Schiavoni, I., Abrignani, S., Antonelli, G., Baldo, V., Baldovin, T., Bandera, A., Bonura, F., Clerici, P.*, et al.* (2022). Evaluation of humoral and cellular response to four vaccines against COVID-19 in different age groups: A longitudinal study. Frontiers in immunology *13*, 1021396.

Fooksman, D.R., Schwickert, T.A., Victora, G.D., Dustin, M.L., Nussenzweig, M.C., and Skokos, D. (2010). Development and migration of plasma cells in the mouse lymph node. Immunity *33*, 118-127.

Fowell, D.J., and Kim, M. (2021). The spatio-temporal control of effector T cell migration. Nat Rev Immunol *21*, 582-596.

Frasca, D., and Blomberg, B.B. (2020). Aging induces B cell defects and decreased antibody responses to influenza infection and vaccination. Immun Ageing *17*, 37.

Gires, O., Pan, M., Schinke, H., Canis, M., and Baeuerle, P.A. (2020). Expression and function of epithelial cell adhesion molecule EpCAM: where are we after 40 years? Cancer Metastasis Rev *39*, 969-987.

Good-Jacobson, K.L., O'Donnell, K., Belz, G.T., Nutt, S.L., and Tarlinton, D.M. (2015). c-Myb is required for plasma cell migration to bone marrow after immunization or infection. The Journal of experimental medicine *212*, 1001-1009.

Greenbaum, D., Colangelo, C., Williams, K., and Gerstein, M. (2003). Comparing protein abundance and mRNA expression levels on a genomic scale. Genome Biol *4*, 117.

Hauser, A.E., Debes, G.F., Arce, S., Cassese, G., Hamann, A., Radbruch, A., and Manz, R.A. (2002). Chemotactic responsiveness toward ligands for CXCR3 and CXCR4 is regulated on plasma blasts during the time course of a memory immune response. J Immunol *169*, 1277-1282.

Higgins, B.W., Shuparski, A.G., Miller, K.B., Robinson, A.M., McHeyzer-Williams, L.J., and McHeyzer-Williams, M.G. (2022). Isotype-specific plasma cells express divergent transcriptional programs. Proc Natl Acad Sci U S A *119*, e2121260119.

Jash, A., Zhou, Y.W., Gerardo, D.K., Ripperger, T.J., Parikh, B.A., Piersma, S., Jamwal, D.R., Kiela, P.R., Boon, A.C.M., Yokoyama, W.M.*, et al.* (2019). ZBTB32 restrains antibody responses to murine cytomegalovirus infections, but not other repetitive challenges. Sci Rep *9*, 15257.

Joyner, C.J., Ley, A.M., Nguyen, D.C., Ali, M., Corrado, A., Tipton, C., Scharer, C.D., Mi, T., Woodruff, M.C., Hom, J.*, et al.* (2022). Generation of human long-lived plasma cells by developmentally regulated epigenetic imprinting. Life Sci Alliance *5*.

Kallies, A., Hasbold, J., Tarlinton, D.M., Dietrich, W., Corcoran, L.M., Hodgkin, P.D., and Nutt, S.L. (2004). Plasma cell ontogeny defined by quantitative changes in blimp-1 expression. The Journal of experimental medicine *200*, 967-977.

Koike, T., Fujii, K., Kometani, K., Butler, N.S., Funakoshi, K., Yari, S., Kikuta, J., Ishii, M., Kurosaki, T., and Ise, W. (2023). Progressive differentiation toward the long-lived plasma cell compartment in the bone marrow. The Journal of experimental medicine *220*.

Lam, W.Y., Jash, A., Yao, C.H., D'Souza, L., Wong, R., Nunley, R.M., Meares, G.P., Patti, G.J., and Bhattacharya, D. (2018). Metabolic and Transcriptional Modules Independently Diversify Plasma Cell Lifespan and Function. Cell reports *24*, 2479-2492 e2476.

Lammermann, T., and Kastenmuller, W. (2019). Concepts of GPCR-controlled navigation in the immune system. Immunological reviews *289*, 205-231.

Lemke, A., Kraft, M., Roth, K., Riedel, R., Lammerding, D., and Hauser, A.E. (2016). Long-lived plasma cells are generated in mucosal immune responses and contribute to the bone marrow plasma cell pool in mice. Mucosal Immunol *9*, 83-97.

Lex, A., Gehlenborg, N., Strobelt, H., Vuillemot, R., and Pfister, H. (2014). UpSet: Visualization of Intersecting Sets. IEEE Trans Vis Comput Graph *20*, 1983-1992.

Li, B., and Dewey, C.N. (2011). RSEM: accurate transcript quantification from RNA-Seq data with or without a reference genome. BMC Bioinformatics *12*, 323.

Lino, A.C., Dang, V.D., Lampropoulou, V., Welle, A., Joedicke, J., Pohar, J., Simon, Q., Thalmensi, J., Baures, A., Fluhler, V., *et al.* (2018). LAG-3 Inhibitory Receptor Expression Identifies Immunosuppressive Natural Regulatory Plasma Cells. Immunity *49*, 120-133 e129.

Liu, X., Yao, J., Zhao, Y., Wang, J., and Qi, H. (2022). Heterogeneous plasma cells and long-lived subsets in response to immunization, autoantigen and microbiota. Nature immunology *23*, 1564-1576.

Madisen, L., Zwingman, T.A., Sunkin, S.M., Oh, S.W., Zariwala, H.A., Gu, H., Ng, L.L., Palmiter, R.D., Hawrylycz, M.J., Jones, A.R., *et al.* (2010). A robust and high-throughput Cre reporting and characterization system for the whole mouse brain. Nat Neurosci *13*, 133-140.

Manz, R.A., Thiel, A., and Radbruch, A. (1997). Lifetime of plasma cells in the bone marrow. Nature *388*, 133-134.

Mathis, D., and Benoist, C. (2009). Aire. Annu Rev Immunol *27*, 287-312.

Mayer, C.T., Gazumyan, A., Kara, E.E., Gitlin, A.D., Golijanin, J., Viant, C., Pai, J., Oliveira, T.Y., Wang, Q., Escolano, A., *et al.* (2017). The microanatomic segregation of selection by apoptosis in the germinal center. Science *358*.

McCarron, M.J., Park, P.W., and Fooksman, D.R. (2017). CD138 mediates selection of mature plasma cells by regulating their survival. Blood *129*, 2749-2759.

Mokhtari, Z., Mech, F., Zehentmeier, S., Hauser, A.E., and Figge, M.T. (2015). Quantitative image analysis of cell colocalization in murine bone marrow. Cytometry A *87*, 503-512.

Nie, Y., Waite, J., Brewer, F., Sunshine, M.J., Littman, D.R., and Zou, Y.R. (2004). The role of CXCR4 in maintaining peripheral B cell compartments and humoral immunity. The Journal of experimental medicine *200*, 1145-1156.

Nunez, S., Moore, C., Gao, B., Rogers, K., Hidalgo, Y., Del Nido, P.J., Restaino, S., Naka, Y., Bhagat, G., Madsen, J.C., *et al.* (2016). The human thymus perivascular space is a functional niche for viral-specific plasma cells. Sci Immunol *1*.

Palacios-Pedrero, M.A., Osterhaus, A., Becker, T., Elbahesh, H., Rimmelzwaan, G.F., and Saletti, G. (2021). Aging and Options to Halt Declining Immunity to Virus Infections. Frontiers in immunology *12*, 681449.

Phan, T.G., Paus, D., Chan, T.D., Turner, M.L., Nutt, S.L., Basten, A., and Brink, R. (2006). High affinity germinal center B cells are actively selected into the plasma cell compartment. The Journal of experimental medicine *203*, 2419-2424.

Pioli, P.D., Casero, D., Montecino-Rodriguez, E., Morrison, S.L., and Dorshkind, K. (2019). Plasma Cells Are Obligate Effectors of Enhanced Myelopoiesis in Aging Bone Marrow. Immunity *51*, 351-366 e356.

Racine, R., McLaughlin, M., Jones, D.D., Wittmer, S.T., MacNamara, K.C., Woodland, D.L., and Winslow, G.M. (2011). IgM production by bone marrow plasmablasts contributes to long-term protection against intracellular bacterial infection. J Immunol *186*, 1011-1021.

Robinson, M.J., Dowling, M.R., Pitt, C., O'Donnell, K., Webster, R.H., Hill, D.L., Ding, Z., Dvorscek, A.R., Brodie, E.J., Hodgkin, P.D., *et al.* (2022). Long-lived plasma cells accumulate in the bone marrow at a constant rate from early in an immune response. Sci Immunol *7*, eabm8389.

Robinson, M.J., Webster, R.H., and Tarlinton, D.M. (2020). How intrinsic and extrinsic regulators of plasma cell survival might intersect for durable humoral immunity. Immunological reviews *296*, 87-103.

Schaum, N., Lehallier, B., Hahn, O., Palovics, R., Hosseinzadeh, S., Lee, S.E., Sit, R., Lee, D.P., Losada, P.M., Zardeneta, M.E., *et al.* (2020). Ageing hallmarks exhibit organ-specific temporal signatures. Nature *583*, 596-602.

Scotton, C.J., Wilson, J.L., Scott, K., Stamp, G., Wilbanks, G.D., Fricker, S., Bridger, G., and Balkwill, F.R. (2002). Multiple actions of the chemokine CXCL12 on epithelial tumor cells in human ovarian cancer. Cancer research *62*, 5930-5938.

Shi, W., Liao, Y., Willis, S.N., Taubenheim, N., Inouye, M., Tarlinton, D.M., Smyth, G.K., Hodgkin, P.D., Nutt, S.L., and Corcoran, L.M. (2015). Transcriptional profiling of mouse B cell terminal differentiation defines a signature for antibody-secreting plasma cells. Nature immunology *16*, 663-673.

Slifka, M.K., Antia, R., Whitmire, J.K., and Ahmed, R. (1998). Humoral immunity due to long-lived plasma cells. Immunity *8*, 363-372.

Srinivas, S., Watanabe, T., Lin, C.S., William, C.M., Tanabe, Y., Jessell, T.M., and Costantini, F. (2001). Cre reporter strains produced by targeted insertion of EYFP and ECFP into the ROSA26 locus. BMC Dev Biol *1*, 4.

Sze, D.M., Toellner, K.M., Garcia de Vinuesa, C., Taylor, D.R., and MacLennan, I.C. (2000). Intrinsic constraint on plasmablast growth and extrinsic limits of plasma cell survival. The Journal of experimental medicine *192*, 813-821.

Takahashi, Y., Dutta, P.R., Cerasoli, D.M., and Kelsoe, G. (1998). In situ studies of the primary immune response to (4-hydroxy-3-nitrophenyl)acetyl. V. Affinity maturation develops in two stages of clonal selection. The Journal of experimental medicine *187*, 885-895.

Utley, A., Chavel, C., Lightman, S., Holling, G.A., Cooper, J., Peng, P., Liu, W., Barwick, B.G., Gavile, C.M., Maguire, O., *et al.* (2020). CD28 Regulates Metabolic Fitness for Long-Lived Plasma Cell Survival. Cell reports *31*, 107815.

Vergani, S., Muleta, K.G., Da Silva, C., Doyle, A., Kristiansen, T.A., Sodini, S., Krausse, N., Montano, G., Kotarsky, K., Nakawesi, J., *et al.* (2022). A self-sustaining layer of early-life-origin B cells drives steady-state IgA responses in the adult gut. Immunity *55*, 1829-1842 e1826.

Wagner, A., and Weinberger, B. (2020). Vaccines to Prevent Infectious Diseases in the Older Population: Immunological Challenges and Future Perspectives. Frontiers in immunology *11*, 717.

Weisel, F.J., Zuccarino-Catania, G.V., Chikina, M., and Shlomchik, M.J. (2016). A Temporal Switch in the Germinal Center Determines Differential Output of Memory B and Plasma Cells. Immunity *44*, 116-130.

Wilmore, J.R., Gaudette, B.T., Gomez Atria, D., Hashemi, T., Jones, D.D., Gardner, C.A., Cole, S.D., Misic, A.M., Beiting, D.P., and Allman, D. (2018). Commensal Microbes Induce Serum IgA Responses that Protect against Polymicrobial Sepsis. Cell Host Microbe *23*, 302-311 e303.

Winkelmann, R., Sandrock, L., Porstner, M., Roth, E., Mathews, M., Hobeika, E., Reth, M., Kahn, M.L., Schuh, W., and Jack, H.M. (2011). B cell homeostasis and plasma cell homing controlled by Kruppel-like factor 2. Proc Natl Acad Sci U S A *108*, 710-715.

Xu, A.Q., Barbosa, R.R., and Calado, D.P. (2020). Genetic timestamping of plasma cells in vivo reveals tissue-specific homeostatic population turnover. eLife *9*.

Zehentmeier, S., and Pereira, J.P. (2019). Cell circuits and niches controlling B cell development. Immunological reviews *289*, 142-157.

1100

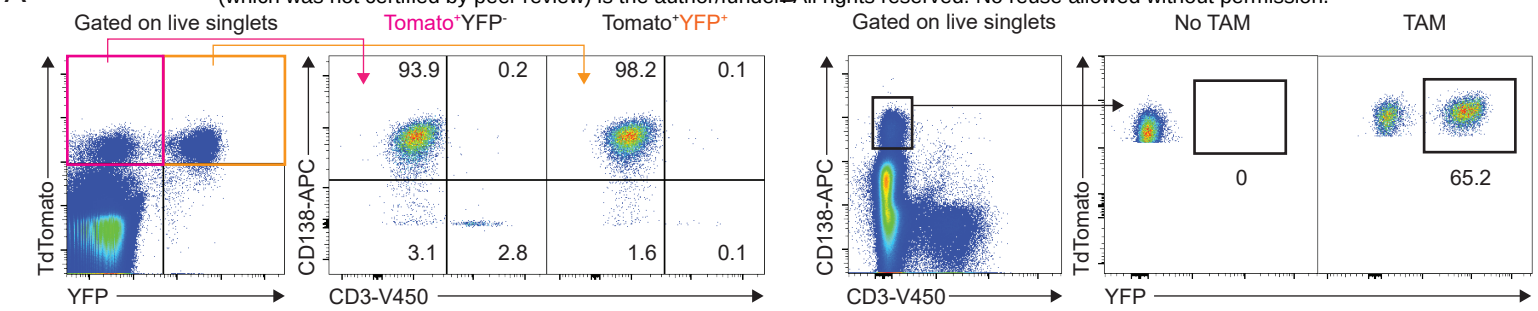

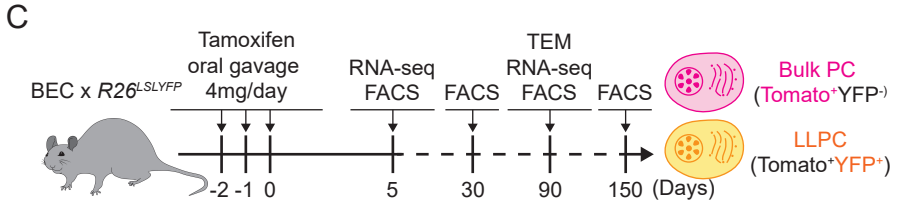

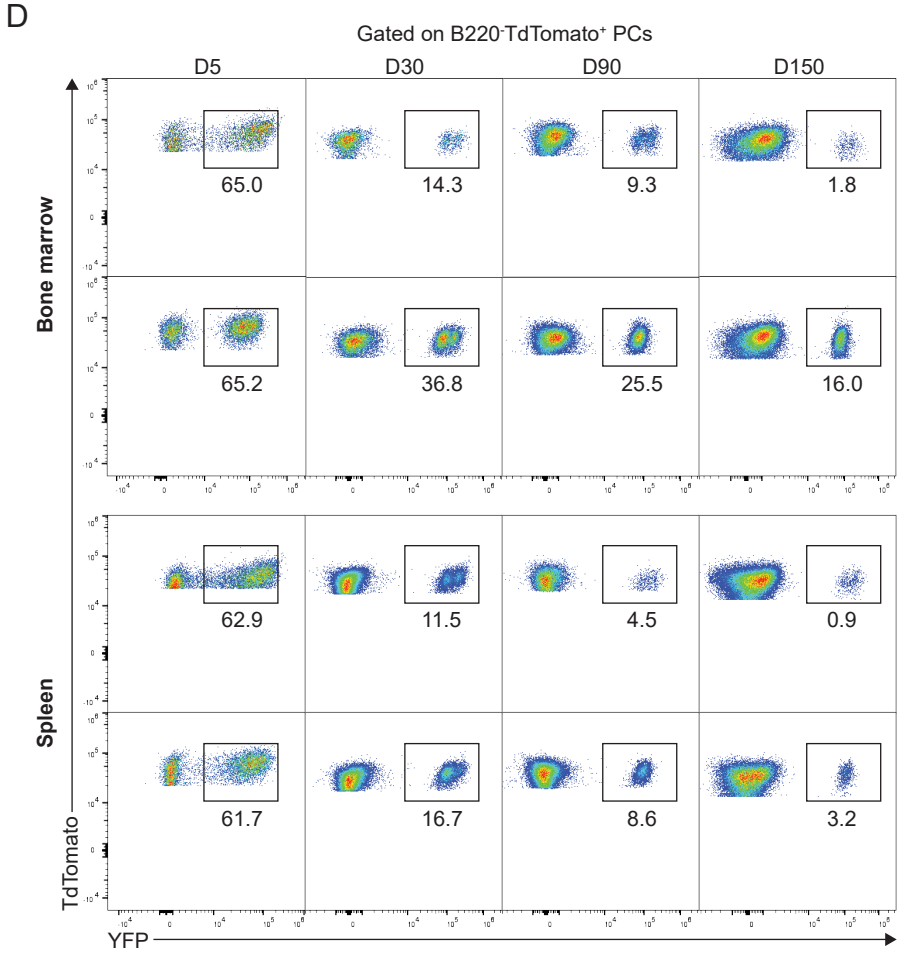

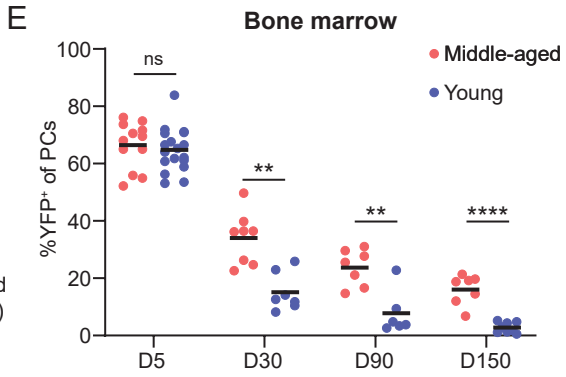

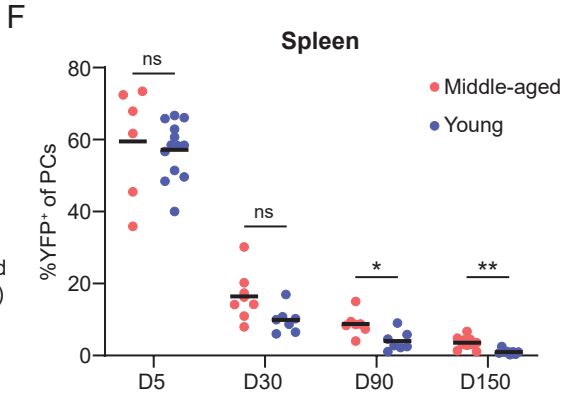

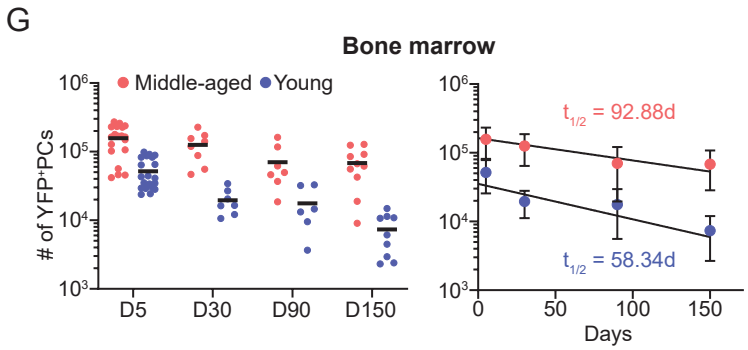

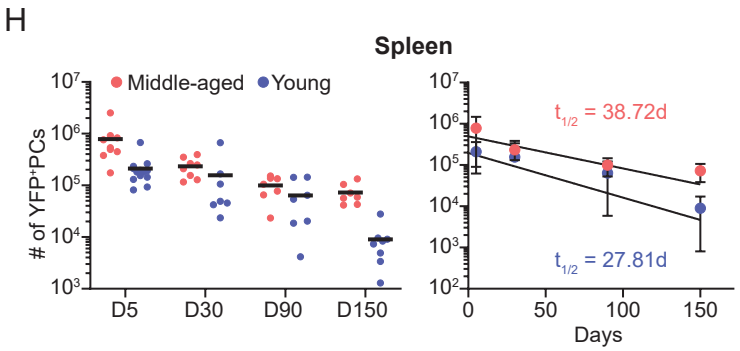

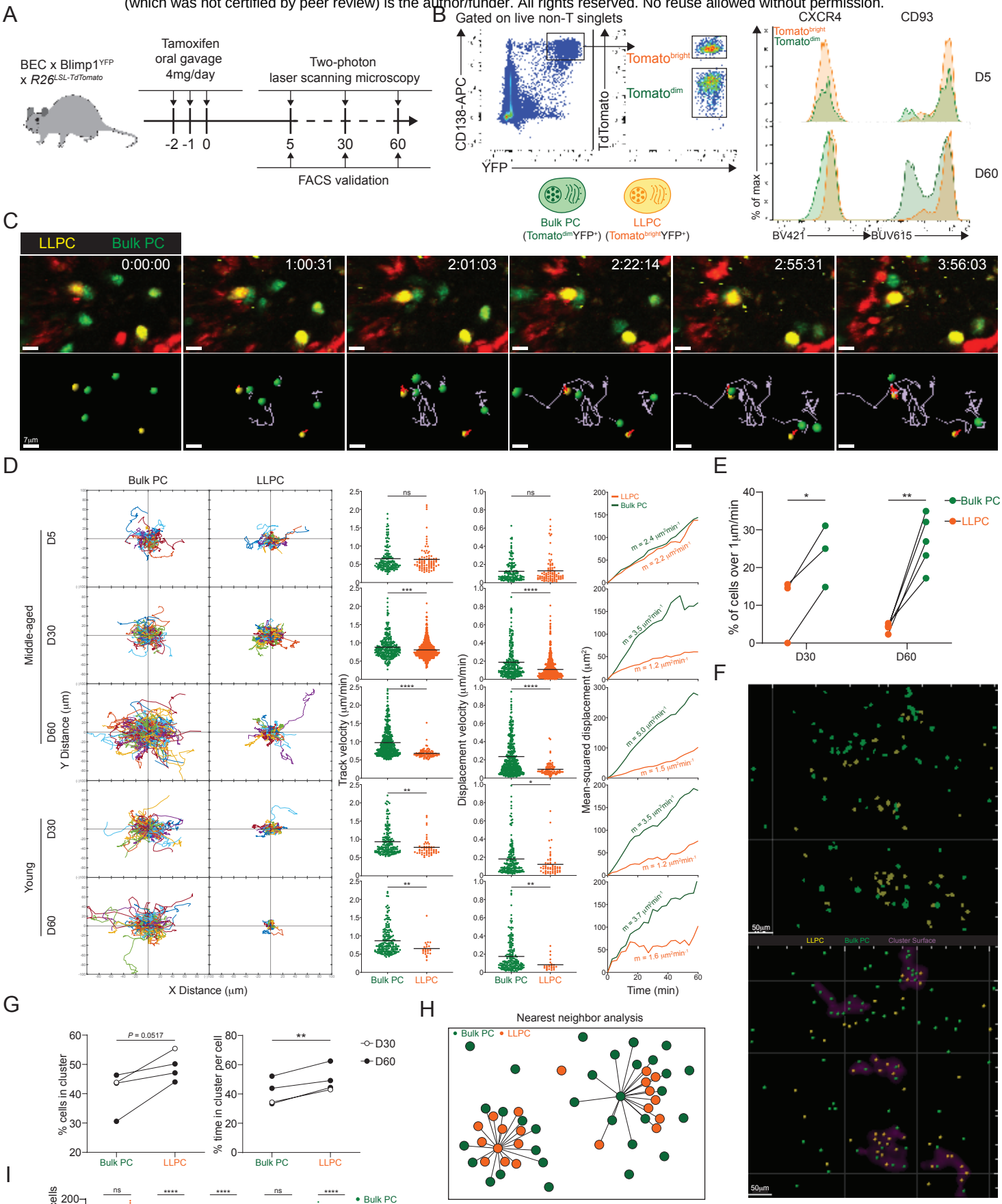

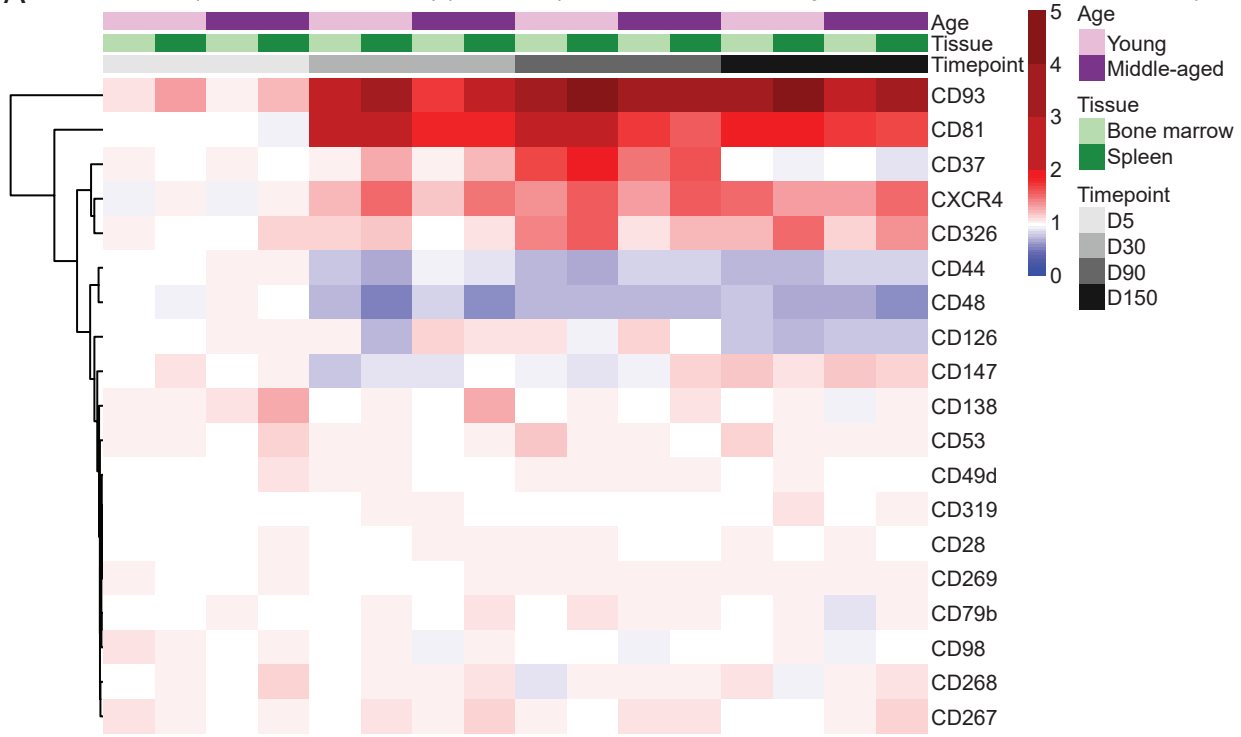

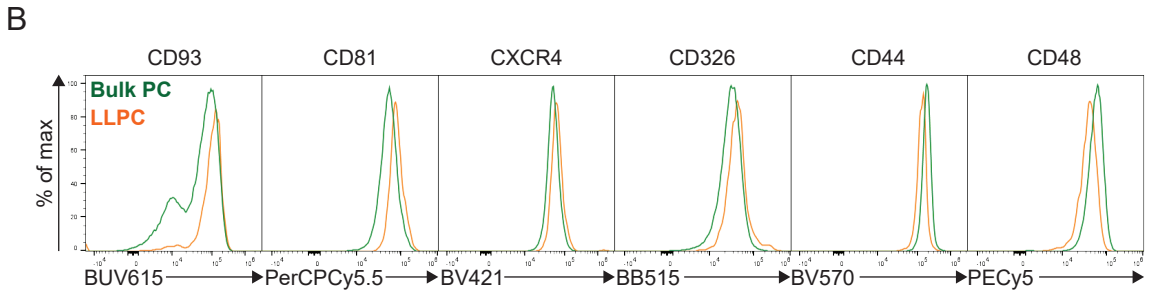

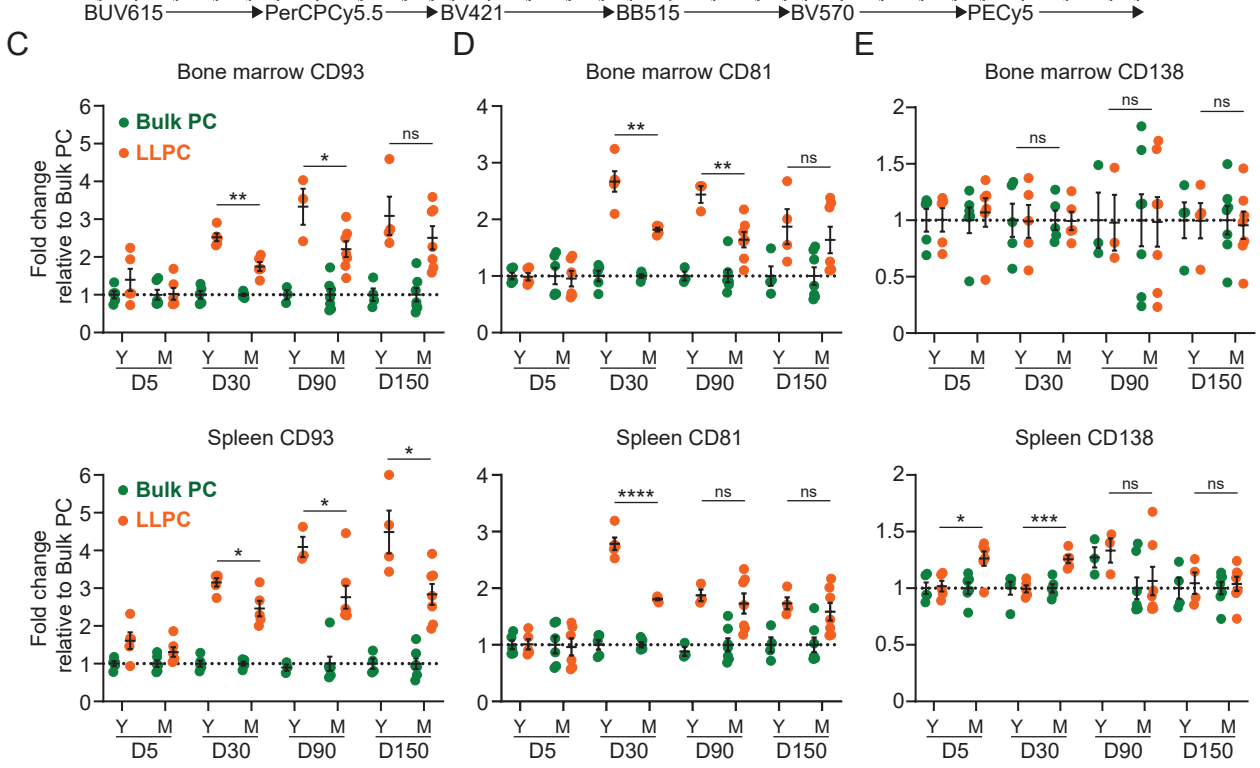

A

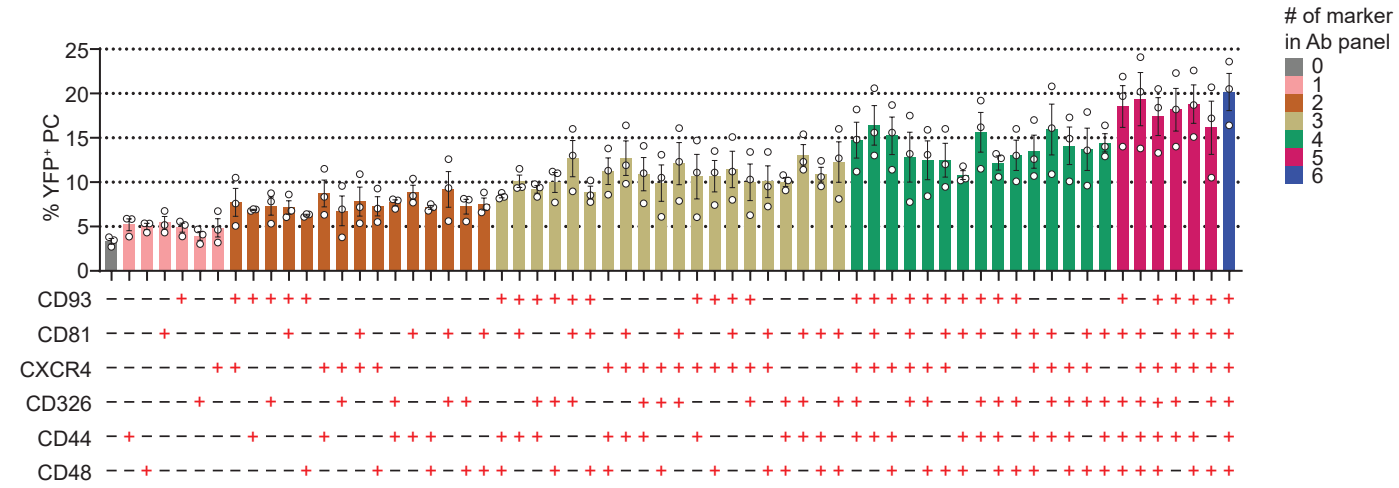

B

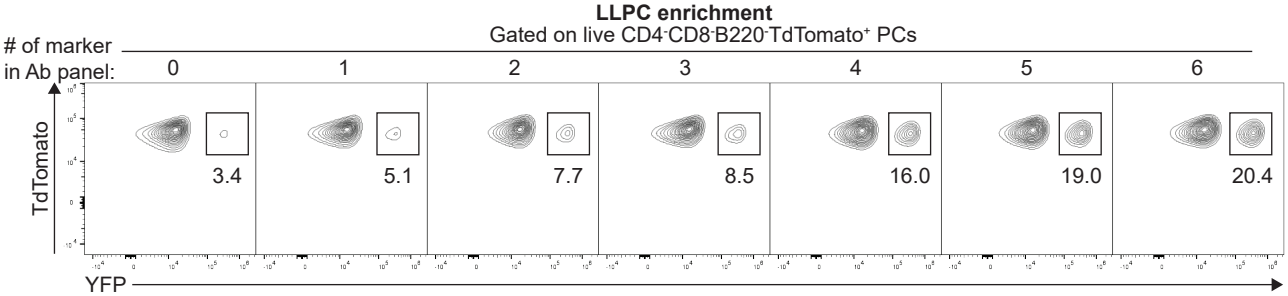

C

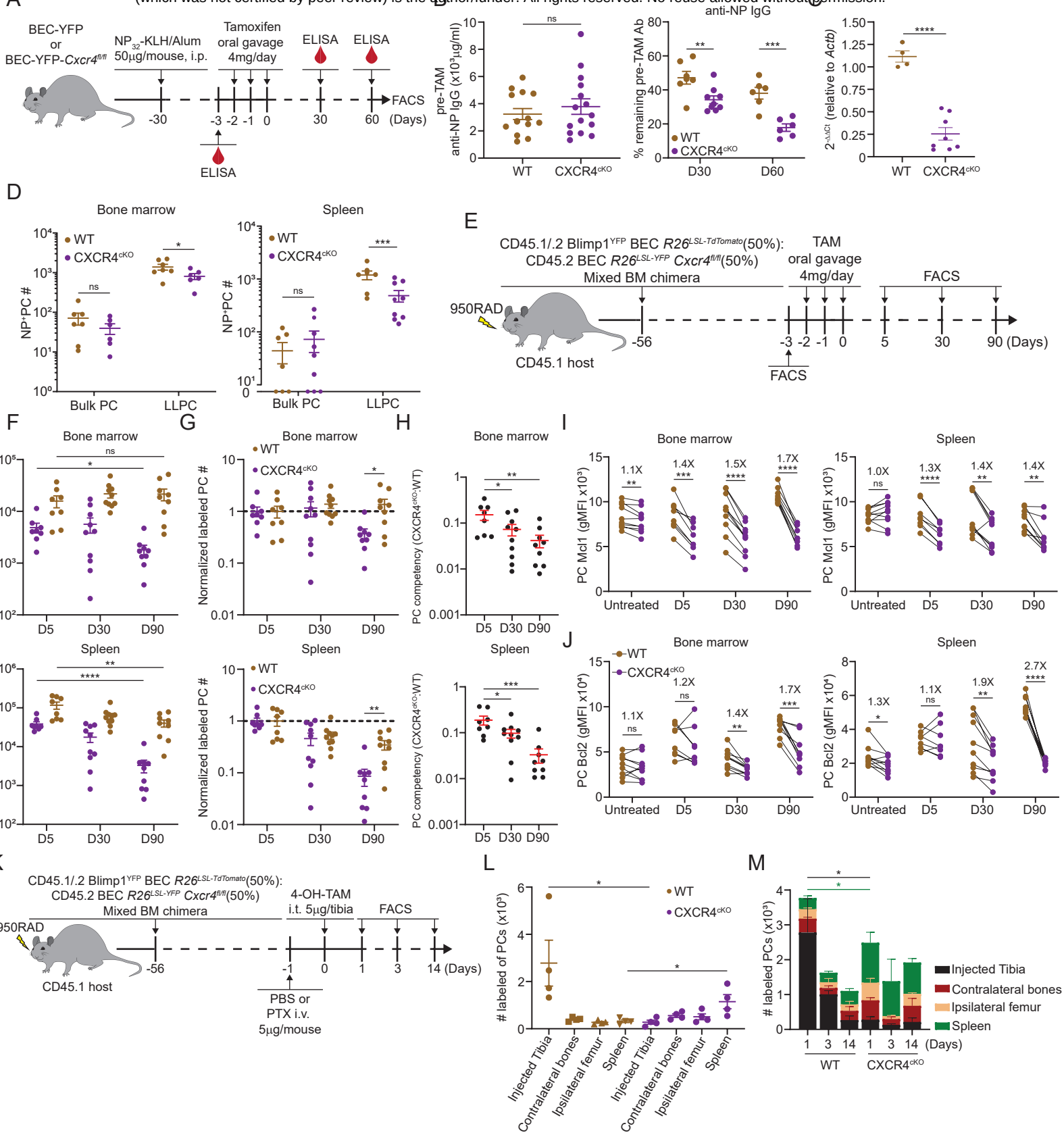

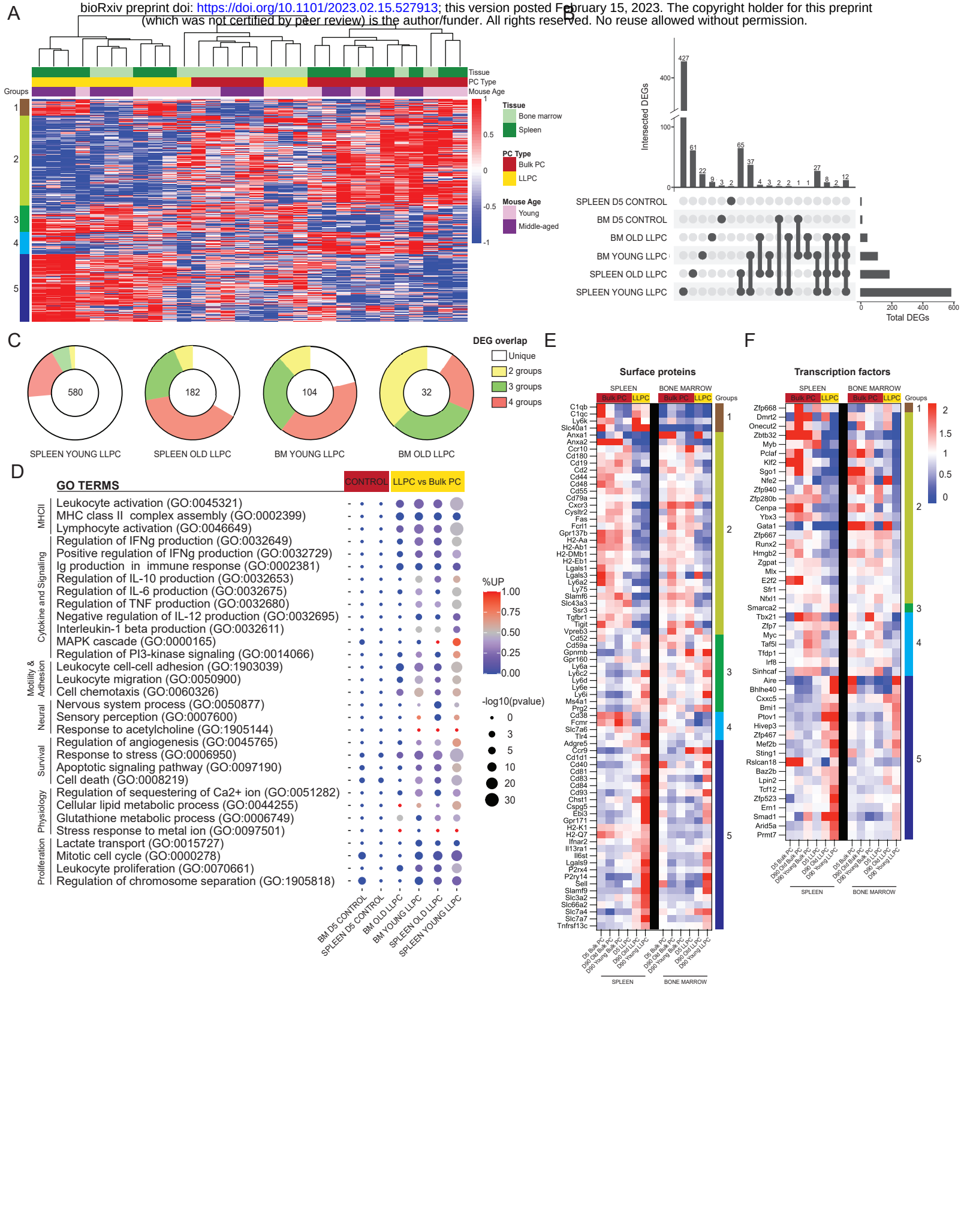

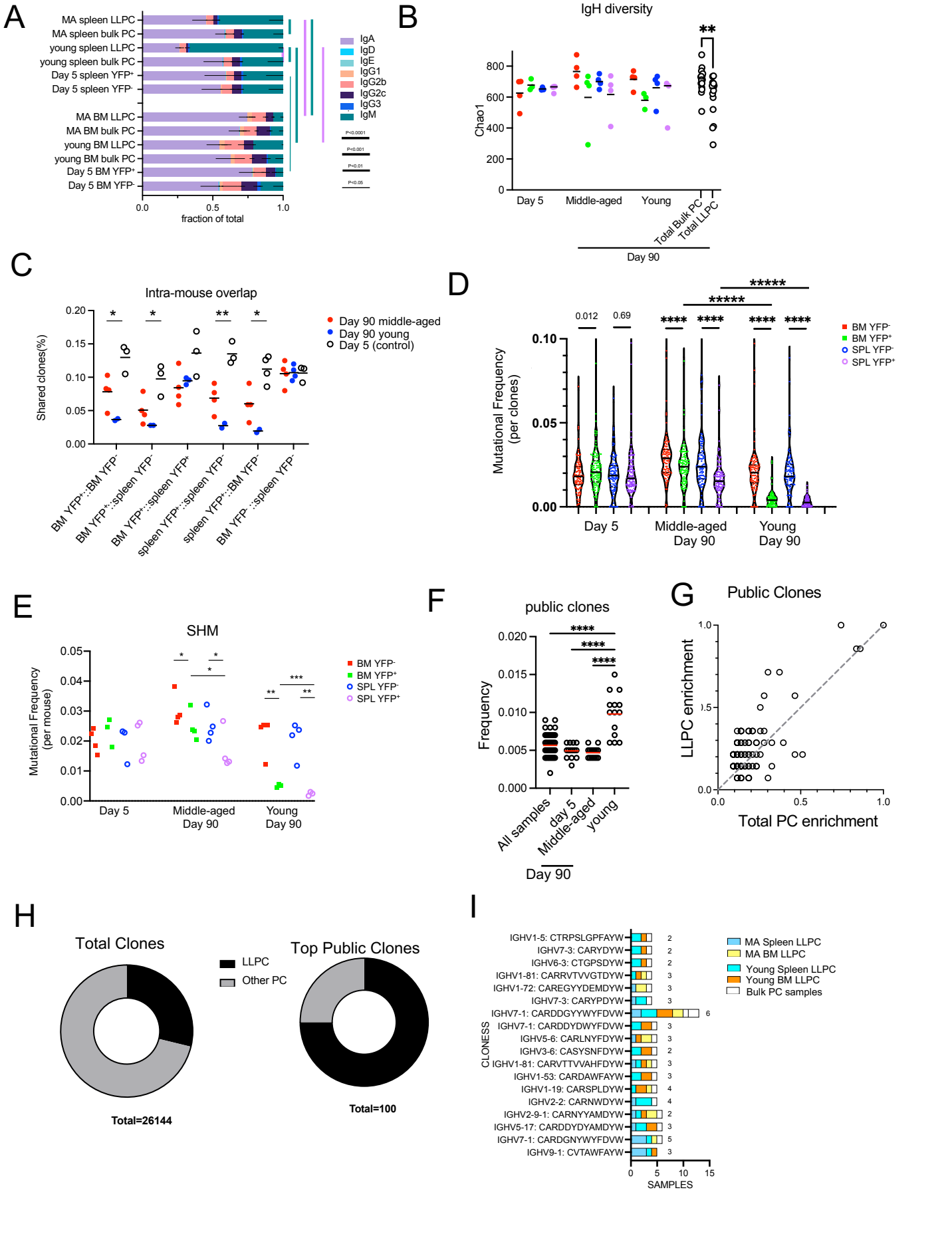
A
MA spleen LLPC
MA spleen bulk PC
young spleen LLPC
young spleen bulk PC
Day 5 spleen YFP+
Day 5 spleen YFP-
MA BM LLPC
MA BM bulk PC
young BM LLPC
young BM bulk PC
Day 5 BM YFP+
Day 5 BM YFP-
0.0
0.5
1.0
fraction of total
IgA
IgD
IgE
IgG1
IgG2b
IgG2c
IgG3
IgM
P<0.0001
P<0.001
P<0.01
P<0.05
B
IgH diversity
Chao1
800
600
400
200
0
**
Day 5
Middle-aged
Young
Total Bulk PC
Total LLPC
Day 90
C
Intra-mouse overlap
Shared clones(%)
0.20
0.15
0.10
0.05
0.00
*
*
**
*
Day 90 middle-aged
Day 90 young
Day 5 (control)
BM YFP+::BM YFP-
BM YFP+::spleen YFP-
BM YFP+::spleen YFP+
spleen YFP+::spleen YFP-
spleen YFP+::BM YFP-
BM YFP- ::spleen YFP-
D
*****
*****
0.012
0.69
****
****
****
****
Mutational Frequency
(per clones)
0.10
0.05
0.00
BM YFP-
BM YFP+
SPL YFP-
SPL YFP+
Day 5
Middle-aged
Day 90
Young
Day 90
E
SHM
Mutational Frequency
(per mouse)
0.05
0.04
0.03
0.02
0.01
0.00
*
*
*
**
**
***
BM YFP-
BM YFP+
SPL YFP-
SPL YFP+
Day 5
Middle-aged
Day 90
Young
Day 90
F
public clones
Frequency
0.020
0.015
0.010
0.005
0.000
****
****
****
All samples
day 5
Middle-aged
young
Day 90
G
Public Clones
LLPC enrichment
1.0
.5
0.0
0.0
0.5
1.0
Total PC enrichment
H
Total Clones
LLPC
Other PC
Total=26144
Top Public Clones
Total=100
I
IGHV1-5: CTRPSLGPFAYW
IGHV7-3: CARYDYW
IGHV6-3: CTGPSDYW
IGHV1-81: CARRVTVVGTDYW
IGHV1-72: CAREGYYDEMDYW
IGHV7-3: CARYPDYW
IGHV7-1: CARDDGYYWYFDVW
IGHV7-1: CARDDYDWYFDVW
IGHV5-6: CARLNYFDYW
IGHV3-6: CASYSNFDYW
IGHV1-81: CARVTTVVAHFDYW
IGHV1-53: CARDAWFAYW
IGHV1-19: CARSPLDYW
IGHV2-2: CARNWDYW
IGHV2-9-1: CARNYYAMDYW
IGHV5-17: CARDDYDYAMDYW
IGHV7-1: CARDGNYWYFDVW
IGHV9-1: CVTAWFAYW
2
2
2
3
3
3
6
3
3
2
3
3
4
4
2
3
5
3
CLONESS
0
5
10
15
SAMPLES
MA Spleen LLPC
MA BM LLPC
Young Spleen LLPC
Young BM LLPC
Bulk PC samples